

Hemichelation, a Way To Stabilize Electron-Unsaturated Complexes: The Case of T-Shaped Pd and Pt Metallacycles.

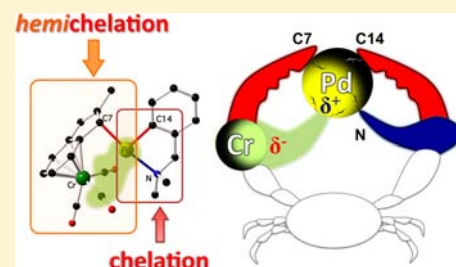
Christophe Werlé, Corinne Bailly, Lydia Karmazin-Brelot, Xavier-Frédéric Le Goff, Louis Ricard, and Jean-Pierre Djukic*

Institut de Chimie de Strasbourg, Université de Strasbourg, CNRS, 4 rue Blaise Pascal, F-67000 Strasbourg, France

Département de Chimie, Ecole Polytechnique, CNRS, Route de Saclay, F-91128 Palaiseau cedex, France

S Supporting Information

ABSTRACT: A rational method of synthesis of stable neutral T-shaped 14 electron Pd and Pt complexes is proposed. It takes advantage of the ambiphilic character of the tricarbonyl(η^6 -indenyl)chromium anion, of which the main property is to behave as a *hemichelating* ligand, that is a nonconventional heteroditopic ligand capable of chelating a metal center by way of covalent and noncovalent bonding, thus preserving its unsaturated valence shell. The reaction of the *in situ* formed tricarbonyl(η^6 -2-methylindenyl)chromium anion with a series of Pd and Pt metallacycles afforded new air-stable and persistent synfacial heterobimetallic complexes in which the metallacycle binds the indenyl fragment via its metal in an η^1 fashion, leaving the fourth coordination site at the chelated metal virtually vacant. The structures of eight of these novel complexes are disclosed, and their bonding features are investigated by an array of theoretical methods based on the density functional theory (NBO, EDA, ETS-NOCV, AIM, NCI region analysis). Theory shows that the formation of these unusual structures of bimetallic synfacial η^1 -indenyl-Pd/Pt complexes is driven thermodynamically by attractive *Coulombic occlusion* of the fourth vacant coordination site at Pd/Pt centers by the $\text{Cr}(\text{CO})_3$ moiety.



1. INTRODUCTION

Coordinatively unsaturated transition metal complexes are thought to take part in a number of catalytic processes as pivotal intermediates.^{1,2} Stabilizing such kinetically unstable species that are electron-unsaturated from the standpoint of the so-called *Sidgwick-Langmuir 18 valence electrons rule*³ represents a great challenge. Persistence can be achieved by using steric occlusion or by promoting labile weak interactions between the metal center and proximal groups of the atoms. Hofmann⁴ showed that labile C–H...M agostic interactions allow the stabilization of unusual d^8 -metal complexes. Along this line, numerous stable models of T-shaped complexes of Pd⁵ and Pt⁶ have been reported. Figueroa's use of bulky alkylisocyanides as ligands of d -transition metals is a good example of how well steric occlusion and cluttering can force the electron-unsaturated metal center into unusual coordination geometries.⁷ Serendipity has offered a host of unusual 16 electron Mn(I) and Re(I) complexes, the structural cohesion of which is thought to stem from a combination of steric cluttering and attractive noncovalent local and nonlocal interactions.⁸ In our continued efforts to analyze the modes of stabilization of electron-deficient centers by noncovalent interactions,^{8,9} a rational method of synthesis of stable neutral T-shaped 14 electron Pd(II) and Pt(II) complexes is now proposed. It takes advantage of the ambiphilic character of the tricarbonyl(η^6 -indenyl)chromium anion, the main property of which is to behave as a nonconventional heteroditopic ligand capable of

chelating a metal center through covalent and noncovalent bonding, thus preserving its unsaturated valence shell.^{9a}

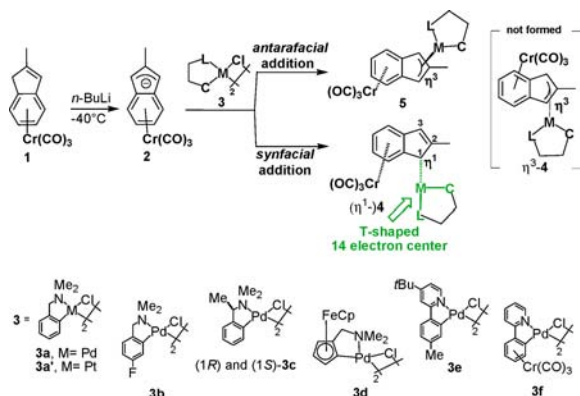
The heteroditopicity of the tricarbonyl(η^6 -2-methylindenyl)-chromium anion was merely outlined in a recent communication^{9a} in which the synthesis of three examples of highly fluxional 14 electron Pd(II) complexes was reported. Those Cr,Pd indenyl complexes had the disadvantage of being air-sensitive and kinetically unstable at room temperature. The present report discloses new cases of air/moisture-stable, solid state, and solution-persistent 14 electron neutral T-shaped Pd(II) and Pt(II) complexes of the η^1 -4 type derived from known metallacycles **3** and from **1** (Scheme 1). This article documents further this peculiar type of chelation, that will be named herein *hemichelation*, where the prefix *hemi* (from the greek $\eta\mu$ meaning *half*) suggests the half covalent/half noncovalent nature of chelation. Theoretical and experimental investigations carried out to establish the physical nature of the intramolecular interactions highlight indeed the stabilizing role of noncovalent interactions.

2. RESULTS AND DISCUSSION

2.1. Synthesis. Several μ -chloro-bridged palladacycles were probed for their reactivity toward anion **2**, anticipating the possible formation of a mixture of syn- and antarafacial products **4** and **5** (Scheme 1). It was observed that only Pd

Received: August 2, 2013

Published: November 1, 2013

Scheme 1^a

^aThe ambiphilic character of anion 2 allows two facial interactions with Pd and Pt metallacycles 3, that is, either the antarafacial leading to the (η^3 -indenyl)M complexes 5 or the synfacial leading exclusively to (η^1 -indenyl)M complexes 4, a new class of electron-unsaturated T-shaped η^1 -indenyl Pd/Pt complexes.

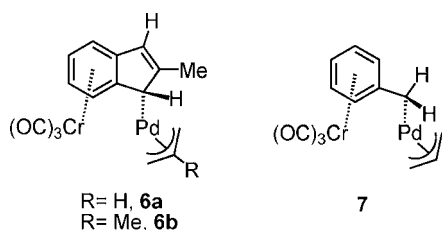
complexes of arylmethylamines (**3a–d**) and 2-arylpyridines (**3e,f**) would yield isolable and air-stable compounds. Optimal conversions were achieved when palladacycles **3a–d**,¹⁰ **3f**,¹⁰ and **3e** reacted with anion 2 in a dry mixture of ether and toluene at -40 °C. The corresponding synfacial complexes **4a–f** were isolated mostly by recrystallization with yields spanning 46–86%. In the case of the reaction of 2 with **3b**, the antarafacial isomer **5b** precipitated out during the course of the reaction, which eased its separation from the synfacial isomer **4b**. However, complex **5b**, which formed in about the same amounts as **4b**, displayed low kinetic stability in solution and generally decomposed within an hour into **1** and other untraceable products. This peculiar instability in solution might explain why no other examples of similar electron-saturated complexes arising from **3a** of **3c–f** were isolated or detected in reaction mixtures, which always displayed typical signs of decomposition (Pd black).

Owing to the poor reactivity of platinumacycle **3a'**¹¹ in organic solvents, slightly forced conditions consisting of a prolonged reaction time with 2 at room temperature had to be applied to produce **4a'** in small amounts in ca. 4% yield. Preliminary conversion of **3a'** into a more reactive intermediary thioether adduct¹² ($\text{Me}_2\text{S}\cdot\text{3a}'$), which was not isolated, slightly improved the yield in **4a'** (12%).

Complexes **4a–f** and **4a'** were air-stable in the solid state and displayed far better kinetic stability in solution in moderately polar solvents than complexes **6a,b** reported earlier^{9a} (Chart 1). Acidic treatment in organic solvents would in all cases regenerate **1** and lead to the decomposition of the palladacycle.

2.2. Structural and Spectroscopic Properties. Structural characterization by means of X-ray diffraction analysis was

Chart 1



successful with complexes **4a–d** and **4f** (Figure 1) as well as with platinum complex **4a'** (Figure 2); being rather insoluble, **4e** failed to yield suitable crystals. Figure 1 displays the structures of the synfacial Cr(0)–Pd(II)/Pt(II) complexes. Table 1 provides a selection of relevant geometric parameters. The Cr–Pd distances are all in the range of 2.84–2.93 Å which is in the approximate range of the sum of empirical van der Waals radii¹³ for Cr (1.4 Å)/Pd (1.4 Å) and Cr/Pt (1.4 Å). The Cr–Pt distance of ca. 2.88 Å in **4a'** (Figure 1b) is shorter by 0.04 Å than the Cr–Pd distance in **4a** (Table 1).

In all structures the chelated Pd or Pt centers are in short contact with one of the vicinal Cr-bound CO ligands and are bonded in a η^1 -fashion to the indenyl ligand. For the sake of clarity, the η^1 -prefix of complexes 4 (Scheme 1) will be omitted in further discussions unless justified for comparison purposes. It is worth noting that for complexes **4d** and **4f**, the planar chiral palladacycles adopt the same orientation in the crystal lattice; the bulky π -bonded metal fragment being placed in the exo position, i.e., away from the indenyl ligand. Structural X-ray diffraction analyses showed in two distinct experiments that crystals of compound (1S)-**4c** (space group $P2_1$, Flack's absolute structure parameter $x = 0.02(5)$) contained the two *endo*-(pS,1S) and *exo*-(pR,1S)-**4c** diastereoisomers in a 1:1 ratio within the unit cell (Figure 1d,e). Compound (1R)-**4c**, which crystallized in the space group $P2_1$ ($x = 0.018(10)$), yielded a crystal containing only the *endo* diastereomer with the absolute configuration (pR,1R) (not displayed here, cf. Supporting Information). The structure of **5b** (Figure 2) presents an unusual dissymmetry of the η^3 -indenyl-Pd bonding which seemingly results from the unbalanced trans influence of the Pd-bound heterochelate via C14 and N1; distance C7–Pd1 is longer than distance C9–Pd1 by ca. 0.2 Å.

Solution (CH_2Cl_2 , CaF_2 cell) and solid state attenuated total reflectance (ATR)-FT-IR spectra of the syn-facial complexes are characterized by the lifted degeneracy of the carbonyl C–O stretching *E* band (the *A* band appears at ca. 1956–1940 cm^{-1}) that gives rise to two distinct bands at ca. 1880 (s) and 1840 (vs) cm^{-1} . This spectroscopic peculiarity characterizes the lack of local C_{3v} symmetry¹⁴ at the $\text{Cr}(\text{CO})_3$ moiety in solution as well as in the solid state. According to DFT calculations of the vibrational modes within the rigid rotor harmonic oscillator (RRHO) approximation for models of η^1 -**4** computed in the gas phase singlet ground state, the band of highest frequency is associated with the “symmetric” elongations of the three C–O bonds of the $\text{Cr}(\text{CO})_3$ moiety. The band of lowest frequency is associated with the “anti-symmetric” elongations of the pseudobridging CO ligand and the CO ligand distant from M (M = Pd, Pt). The midband corresponds to the antisymmetric elongations of the nonbridging CO ligand proximal to M and the CO ligand distant from M. IR spectroscopy suggests that the pseudo-bridging situation observed in the X-ray diffraction structures has a minor electronic influence on the interaction of the M center with the $\text{Cr}(\text{CO})_3$ moiety; in other terms it has no major electronic effect upon the force constants of the considered C–O bonds, the vibrational modes of which remain overall in the spectral region of conventional (η^6 -arene)tricarbonylchromium complexes. The average relative shift $\Delta(\tilde{\nu})_{\text{aver } 4-1}$ to higher reciprocal wavelengths of the considered vibrational bands of **4** with respect to reference compound **1** (A, 1934 cm^{-1} ; E, 1839 cm^{-1} ; $\tilde{\nu}_{\text{aver } 1} = 1870 \text{ cm}^{-1}$) spans +11 to +26 cm^{-1} . For complex **5b**, the local C_{3v} symmetry of the $\text{Cr}(\text{CO})_3$ rotor¹⁴ is preserved: A and E bands of the pseudo- C_{3v} *fac*-tricarbonylmetal moiety

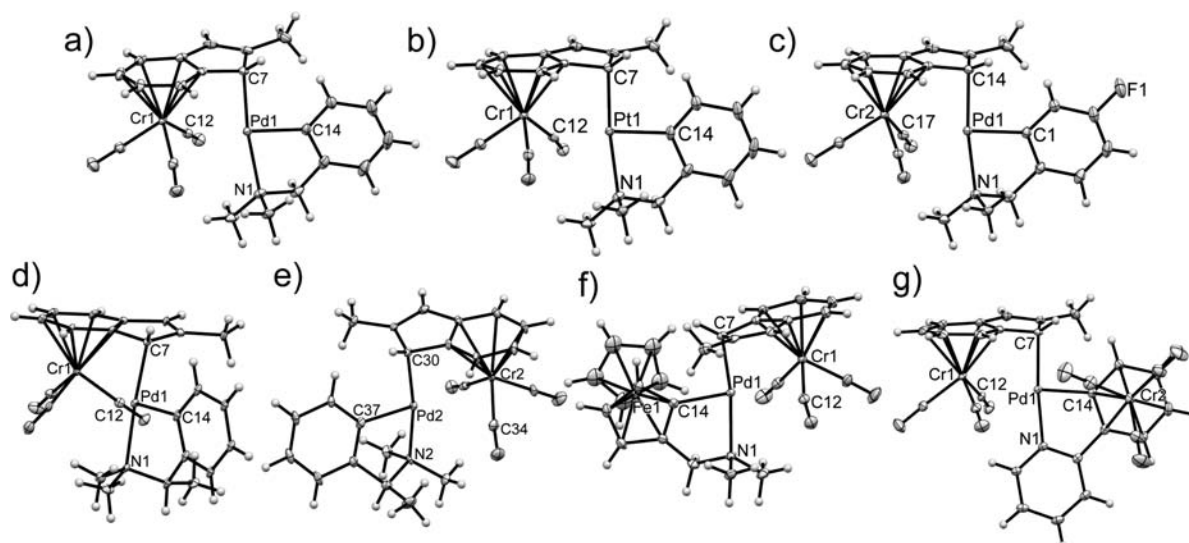


Figure 1. Ellipsoid-type plots of the structures of (a) **4a**, (b) **4a'**, (c) **4b**, (d) *endo*-(*pS,1S*)-**4c**, (e) *exo*-(*pR,1S*)-**4c**, (f) **4d**, and (g) **4f** drawn at the 30% probability level with partial atom numbering. Molecules of solvents were omitted for the sake of clarity.

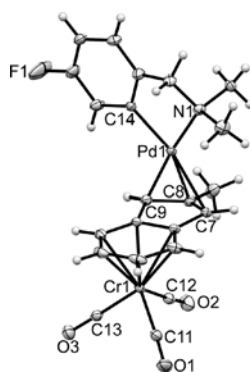


Figure 2. Ellipsoid-type plot of the structure of **5b** at 30% probability level. Selected interatomic distances (in Å) for **5b**: C9–Pd1, 2.161(2); C8–Pd1, 2.189(2); C7–Pd1, 2.350(2); C14–Pd1, 2.010(2); N1–Pd1, 2.109(2).

appear at 1933 (s) and 1843 (broad and vs) cm^{-1} . As far as complex **4c** is concerned, the solid state IR spectrum of either crystalline or amorphous solid obtained by freeze-drying a benzene solution has proved inconclusive as to the possible coexistence of *endo* and *exo* diastereomers in solution; a single set of three vibrational bands being observed.

The room temperature ^{13}C NMR spectra of **4a–f** and **4a'** in d_6 -benzene present the typical signature of a rotation-hindered $\text{Cr}(\text{CO})_3$ moiety in an asymmetric local environment¹⁶ that is materialized by three broad signals at around δ 239, 237, and 235 ppm. All the remaining signals pertaining to the indenyl ligand and the palladacycle are sharp and well resolved.

Given that fluxionality was inherent to complexes **6a,b**, compounds **4** were investigated by conventional dynamic NMR techniques.¹⁷ (The method based on peak separation¹⁷ for the determination of exchange rates in two-state systems was not considered.) Unfortunately, the conventional band shape analysis, Deverell-Morgan-Strange method,^{17,18} EXSY, and polarization transfer experiments proved inconclusive as to the fluxional nature of the new complexes **4** (cf. Supporting Information for discussion). Nonetheless, theory suggested that the energetic barrier to a possible $\eta^1-\eta^3-\eta^1$ transposition^{9a} in complexes **4** might be of the same amplitude as that estimated

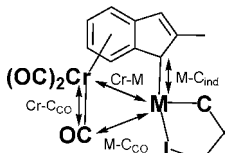
for **6b** in d_8 -toluene.^{9a} In **4a** and **4a'** the differences in Gibbs enthalpy ΔG between the singlet ground states of the respective η^1 states and the η^3 transients amount to, according to DFT calculations, 8.9 and 11.3 kcal/mol (conductor-like screening model (COSMO) toluene, zero order regular approximation (ZORA)-PBE-D3(BJ)/all electron TZP), which suggests that all the new disclosed complexes might well be fluxional in solution.

A few examples are particularly remarkable by their typical ^1H NMR signature. For instance, complex **4f**, which contains a planar-chiral palladacycle, produces a single set of signals in ^1H NMR spectroscopy, whereas theory suggests that the *exo* and *endo*-**4f** isomers corresponding to the two possible positions of the $\text{Cr}(\text{CO})_3$ moiety in the 2-phenylpyridine ligand should be nearly equally populated (Figure 3): theory predicts a *endo*-to-*exo* Gibbs enthalpy of activation difference of ~ 10 kcal/mol for **4f** in the gas phase at 298.15 K.

In this respect, also particularly significant is the case of (*1S*)-**4c**, which contains a chiral moiety, that is, the palladated (*1S*)-*N,N*-dimethyl,1-phenylethylamine ($ee \approx 98\%$) ligand. The room temperature ^1H NMR spectrum of this compound in d_8 -toluene reveals also a single set of signals, a rather ambiguous situation that apparently contradicts the results of structural X-ray diffraction analyses.

The ^1H NMR spectrum of **4c** in d_8 -toluene at room temperature displays the signals of protons H(1) and H(3) (Figure 4) as two distinct singlets at δ 5.6 and 4.4 ppm ($\Delta\delta$ (ppm) = 1.2 ppm). Variable temperature ^1H NMR investigations of the same d_8 -toluene solution of (*1S*)-**4c** at subambient temperatures ($213(1) < T$ (K) $< 298(1)$) did not reveal any significant line-broadening of the signals of H(1) and H(3) upon cooling, which precluded further extraction of thermodynamic parameters from dynamic NMR band shape analysis. Nonetheless, modeling the transposition process by means of the DFT, with an *ad hoc* treatment of solvation in toluene (COSMO ZORA¹⁵-PBE²⁰-D3(BJ)/TZP), revealed a Gibbs enthalpy variation $\Delta G_{\text{theor}}^{298}$ (*endo*- η^1 -**4c**-to-*endo*- η^3 -**4c**) of +7.4 kcal/mol at 298.15 K, that is, by ca. 3–4 kcal/mol lower than the one estimated for **6b**;^{9a} diastereomers *endo* and *exo*-**4c** being practically isoenergetic (Figure 4). In this simplified transposition mechanism, the $\eta^1-\eta^3-\eta^1$ excursion of the

Table 1. Selected Distances (in Å) Taken from Structural X-ray Diffraction Analysis and DFT Calculations at Different Levels of Theory



cmpd/method ^a	Cr–M	M–C _{ind}	M–C _{CO}	Cr–C _{CO}
		4a (M = Pd)		
X-ray diffr. ^b	2.9290(3)	2.1080(15)	2.5720(16)	1.8564(16)
PBE-D3(BJ) ^c	2.852	2.141	2.434	1.863
PBE0-dDsC ^c	2.792	2.123	2.437	1.846
		4a' (M = Pt)		
X-ray diffr.	2.8834(6)	2.099(4)	2.408(4)	1.876 (4)
PBE-D3(BJ) ^c	2.823	2.122	2.212	1.910
TPSS-D3(BJ) ^c	2.807	2.125	2.231	1.914
PBE0-dDsC ^c	2.830	2.095	2.343	1.860
		4b (M = Pd)		
X-ray diffr.	2.9125(4)	2.110(2)	2.605(2)	1.854(2)
PBE-D3(BJ) ^c	2.844	2.143	2.434	1.863
TPSS-D3(BJ) ^c	2.801	2.141	2.420	1.876
PBE0-dDsC ^c	2.790	2.119	2.435	1.845
		<i>endo</i> -(pS,1S)- 4c (M = Pd)		
X-ray diffr.	2.9130(16)	2.114(8)	2.517(10)	1.858(10)
PBE-D3(BJ) ^c	2.894	2.135	2.504	1.859
		<i>exo</i> -(pR,1S)- 4c (M = Pd)		
X-ray diffr.	2.9312(17)	2.115(8)	2.572(11)	1.845(12)
PBE-D3(BJ) ^c	2.905	2.135	2.550	1.855
		4d (M = Pd)		
X-ray diffr.	2.8505(6)	2.111(3)	2.567(3)	1.857(3)
PBE-D3(BJ) ^c	2.815	2.145	2.508	1.857
TPSS-D3(BJ) ^c	2.774	2.146	2.516	1.864
PBE0-dDsC ^d	2.833	2.142	2.494	1.814
		4e (M = Pd)		
PBE-D3(BJ) ^c	2.830	2.146	2.473	1.864
		4f (M = Pd)		
X-ray diffr.	2.8392(6)	2.111(3)	2.515(3)	1.849(3)
PBE-D3(BJ) ^c	2.816	2.138	2.444	1.864

^aAll-electron triple- ζ Slater-type orbital basis sets with one polarization function (TZP) were used throughout this study¹⁵ unless otherwise stated. ^bSee, for example, the Supporting Information for crystallographic information. ^c*Ad-hoc* all electron TZP basis set associated to the scalar relativistic ZORA¹⁵ treatment. ^dAll electron TZP basis set (C,H,N,O, Cr, Fe), frozen core up to 3d level for Pd.¹⁵

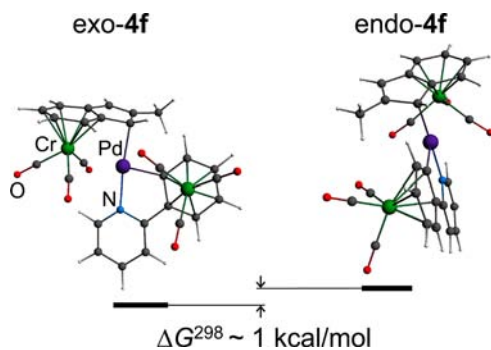


Figure 3. Gas-phase singlet ground-state geometries of the nearly isoenergetic *exo* and *endo*-**4f** diastereomers (ZORA-PBE-D3(BJ)/all electron TZP, $T = 298.15$ K).

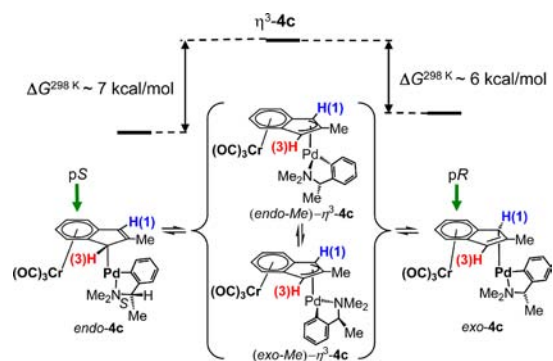


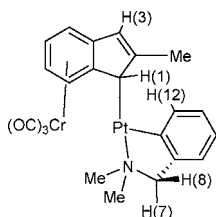
Figure 4. Putative mechanism of transposition of the palladacyclic unit in (1S)-**4c** modeled by DFT (COSMO toluene). Planar chiral configurations are assigned according to Schlögl's convention¹⁹ giving priority $n^{\circ}1$ to the Pd-substituted carbon position.

palladium center at the indenyl ligand (Figure 4) entails two nearly isoenergetic metastable η^3 -**4c** transients in which one

side of the palladacycle faces the $\text{Cr}(\text{CO})_3$ tripod, with the α -Me group pointing either toward (endo orientation) or outward the latter tripod (exo orientation).

The ^1H NMR of **4a'** is characterized by the typical satellite signals arising from the coupling of ^1H nuclei with the ^{195}Pt isotope (33.8% natural abundance, experimental $\delta^{195}\text{Pt} = -2524$ ppm, ZORA-PBE-D3(BJ)/all electron TZP $\delta^{195}\text{Pt} = -2139$ ppm). On the basis of the computed ^{195}Pt -coupled NMR spectrum (COSMO, ZORA-PBE-D3(BJ)/all electron TZP) it was established that signals that bear the strongest ^1H - ^{195}Pt scalar coupling constants in absolute value are those of H(1) ($|J_{\text{exp}}| = 134.7$ Hz, $|J_{\text{theor}}| = 116.8$ Hz), H(12) ($|J_{\text{exp}}| = 74.7$ Hz, $|J_{\text{theor}}| = 65.6$ Hz), H(7) ($|J_{\text{exp}}| = 61.9$ Hz, $|J_{\text{theor}}| = 86.8$ Hz), H(3) ($|J_{\text{exp}}| = 19.6$ Hz, $|J_{\text{theor}}| = 15.6$ Hz) and the methyl groups ($|J_{\text{exp}}| = 31.8$ and 24.0 Hz) (Chart 2). Owing to an

Chart 2. ^1H Nuclei Displaying in **4a'** Significant Scalar Coupling with the ^{195}Pt Nucleus



approximate 90 deg H(8)-C-N-Pt dihedral angle, proton H(8) displays no sensible coupling with the ^{195}Pt nucleus in the experimental spectrum ($|J_{\text{theor}}| = 2.3$ Hz) (Chart 2). It is worth noting that the satellite signals progressively broaden upon lowering the temperature of the NMR probe to eventually vanish at 213 K.

2.3. Chemical Bonding in Synfacial Complexes 4. All experimental geometries of **4** were reproduced acceptably with DFT-D3 methods,²¹ that is, the dispersion-corrected PBE²⁰-D3(BJ^{21b}) and TPSS²²-D3(BJ) functionals, and with the hybrid PBE0-dDsC²³ functional. The methods expectedly^{9a} all gave slightly shorter Cr-M distances as compared to that of crystal-state structures (Table 1), leading to an apparent slight mutual tightening of metal centers and overbinding of the latter with their ligands. The computed geometries of **4** were subsequently analyzed by an array of methods in order to identify the nature of the interactions existing between the $\text{Cr}(\text{CO})_3$ moiety and the M center (M = Pd, Pt) at its fourth vacant coordination site.

Analysis by the Natural Bond Orbital (NBO)²⁴ method established clearly the η^1 mode of coordination of M (M = Pd,

Pt) to the indenyl ligand. The $\text{C}_{\text{indenyl}}\text{-M}$ bonds in models of **4a** and **4a'** bear Wiberg indexes (abbreviation, wbi) of 0.36 and 0.48, respectively, that are relatively lower than those of metallacyclic $\text{C}_{\text{Ar}}\text{-M}$ bonds, which amount to 0.53 and 0.60, respectively. According to the NBO analysis of **4a'**, the hybrid natural orbital at the carbon contributing to the Pt- $\text{C}_{\text{indenyl}}$ bond (Pt-C1 according to atom numbering in Scheme 1, natural bonding orbital population 1.73 e) possesses an overwhelming p character (sp^5) that confines the interaction with the Pt center to a typical σ coordinative bond.²⁵ In the case of **4a**, the NBO analysis, which relies on Lewis structures computed with a bond electron population threshold of 1.5 electron, did not produce any information on the Pd- $\text{C}_{\text{indenyl}}$ interaction due to its formal low electron population. Nonetheless, the neighboring C1-C2 and C2-C3 bonds (cf. numbering in Scheme 1) at the indenyl ligand in **4a** and **4a'** were found to have a single (wbi ~ 1.0) and a double (wbi ~ 1.6) bond character respectively. In **4a**, ^1H - ^{13}C coupling constants for the nuclei at position 1 ($J_{\text{C-H}} = 158$ Hz) and 3 ($J_{\text{C-H}} = 169$ Hz) displayed values similar to those observed in **1** for the CH_2 ($J_{\text{C-H}} = 157$ Hz) and CH ($J_{\text{C-H}} = 167$ Hz) position, respectively, at the five-membered ring, which suggests that C1 has a quasi- sp^3 hybridization.

Inspection of the Wiberg bond indices for the Cr-M (M = Pd, Pt) segment indicated in all addressed cases values close to 0.1, which suggested a very low covalent character for the metal-metal interaction (Table 2). Further the extended transition state-natural orbitals for chemical valence (ETS-NOCV) analysis,²⁶ which provides symmetry-ordered information on the orbital interaction between two closed shell intramolecular fragments, were carried out with a model of **4a**. The mutual interaction of the $\text{Cr}(\text{CO})_3$ moiety with the palladated indenyl ligand was considered and orbital interactions that could be involved in a possible M-Cr($\text{CO})_3$ interaction were identified. Figure 5 displays a selection of four density deformation $\Delta\rho$ plots ordered by decreasing orbital interaction energy for the considered interfragment interaction. One can clearly notice that $\Delta\rho_1$ contains a significant component of electron density donation mostly from the chromium toward the intermetallic space and the palladacycle. $\Delta\rho_3$ contains partly an indirect Pd-to-Cr back-donation component. Most of the orbital interaction in both cases is focused on the build-up of Cr-arene bonds. These two interactions represent less than 50% of the total orbital interaction energy, which amounts to -155.3 kcal/mol. Similar observations can be made for **4a'**.

Table 2. Wiberg Indices for the Cr-M Segment ($\text{wbi}(\text{Cr-M})$ M = Pd, Pt) and Natural Charges (q , Natural Population Analysis) at the $\text{Cr}(\text{CO})_3$ Moiety in a Series of Gas-Phase Singlet Ground State Models

	1	4a	4a'	6a	$\eta^1\text{-4b}$	$\eta^3\text{-4b}$	5b
$q(\text{Cr})$	-0.86	-0.84	-0.82	-0.82	-0.84	-0.81	-0.82
$q(\text{C}_{\text{CO-Pd}})$	+0.60 ^a	+0.59	+0.53	+0.59	+0.59	+0.63 ^b	+0.65 ^a
$q(\text{Cr}(\text{CO})_3)$	-0.27	-0.39	-0.46	-0.34	-0.39	-0.34	-0.27
$\Delta q[\text{Cr}(\text{CO})_3]^c$		-0.12	-0.19	-0.07	-0.12	-0.07	0.00
$q(\text{M})$		+0.59 ^d	+0.59 ^e	+0.60 ^d	+0.60 ^d	+0.68 ^d	+0.64 ^d
$\Delta q(\text{M})^f$		+0.03	+0.13	-0.03	+0.04	+0.02	-0.01
wbi(Cr-M)		0.1 ^d	0.1 ^e	0.1 ^d	0.1 ^d	0.0 ^d	0.0 ^d

^aAveraged value. ^bCalculated for the shortest $\text{C}_{\text{CO}}\text{-Pd}$ distance (3.20 Å). ^c $\Delta q[\text{complex}, \text{Cr}(\text{CO})_3] = q[\text{compound}, \text{Cr}(\text{CO})_3] - q[\text{1}, \text{Cr}(\text{CO})_3]$. ^dM = Pd. ^eM = Pt. ^f $\Delta q(\text{M}) = q(\text{M})_{\text{compound}} - q(\text{M})_{\text{prepared fragment}}$ where the prepared fragment is the metalated indenyl ligand in its prepared geometry prior to interaction with the prepared $\text{Cr}(\text{CO})_3$ moiety.

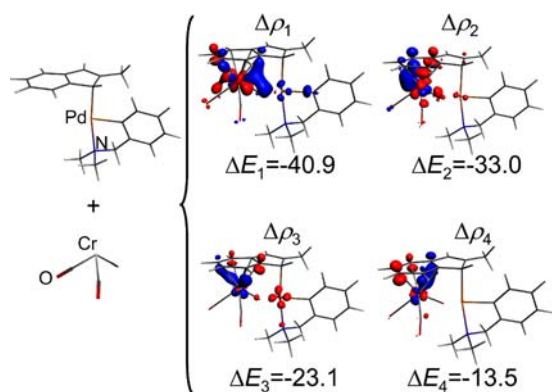


Figure 5. ETS-NOCV deformation densities $\Delta\rho$ and their stabilization energy ΔE^{ob} (in kcal/mol) for the interaction of prepared $\text{Cr}(\text{CO})_3$ and palladated indenyl fragments of **4a**. Red and blue-colored isosurfaces materialize regions where charge density depletion and build up occur respectively: electron density transfer operates from red-colored areas to blue ones upon bonding. Deformation density isosurface contour was set to 0.005 e/bohr.³

Qualitative information on the electronic influence of the metallacycle onto the $\text{Cr}(\text{CO})_3$ moiety was gained by an inspection of the sum of natural charges²⁴ at the $\text{Cr}(\text{CO})_3$ tripod of **4a**, **4a'**, and **4b**, i.e. $q[\text{Cr}(\text{CO})_3]$. Worthy of note, the Cr and the M (M = Pd, Pt) centers display marked negative and positive natural charges (Table 2). Natural charges reflect, in an atom-wise manner, the molecular distribution of charge densities, and may provide basic information on the redistribution of electron density. For instance, the electronic effect of the Pd/Pt center bound to the indenyl ligand was evaluated by the deviation $\Delta q[\text{Cr}(\text{CO})_3]$ of the sum of charges born by the $\text{Cr}(\text{CO})_3$ moiety in a given complex by comparison to a reference compound, that is, **1**, where the benzylic position is occupied by two hydrogen atoms. The negative charge increase apparent from Table 2 for all complexes **4** ($\Delta q[\text{Cr}(\text{CO})_3] \approx -0.15$) is accompanied with a slight increase of the positive natural charge at M (M = Pd, Pt). It is speculated that this relative overall electron density enrichment at the tripod of **4** is slightly compensated by the $(\text{CO})_3\text{Cr} \rightarrow \text{Pd}$ donor-acceptor interaction embodied by $\Delta\rho_1$ (Figure 5), which may explain the slight shift to higher frequency relative to **1** observed for the IR signature of the carbonyl stretching bands of **4**.

Given the low Wiberg indices of the M–Cr segment, further analyses with Bader's *Quantum Theory of Atoms in Molecule* (QTAIM)²⁷ were carried out with a selected group of models in order to clarify the weight of covalence in the M–Cr(CO)₃ interaction. Several cases displaying rather different computed Cr–M distances were considered. These are namely **4a**, **4a'**, **4b**, and **4d**, the geometries of which were optimized with the hybrid PBE0²⁸ functional to which a dDsC²⁹ density-dependent correction for mid-to-long-range dispersion is appended (Table 1). The absence of electron density topological *bond critical point* (BCP) and bond path in the Cr–M segment, that is, two sufficient conditions to rule out the existence of a covalent Cr–metal bond according to Bader's QTAIM criteria, was established in all cases. The only feature related to some direct interaction of M with the $\text{Cr}(\text{CO})_3$ fragment was a recurrent BCP(3,-1) located in between the M (M = Pd, Pt) center and the vicinal pseudobridging carbon atom of the carbonyl ligand for models of **4b** and **4d**. In both cases, this BCP ($\rho = 0.050$ au, $L = -0.0297$ au, and $\rho = 0.044$ au, $L = -0.0268$ au respectively)

localized in the Pd1–C17 and the Pd1–C12 bond paths (Figure 1) fullfills the criteria of a weak closed-shell van der Waals interaction (Wiberg indice ≈ 0.2) according to Popelier.^{27b} Compared to other cases where carbonyl bridges are characterized by at least 5-to-10-fold larger values of electron density population ρ at the BCP, as in tetracobalt clusters³⁰ and nonacarbonyliron³¹ complexes, the CO bridge described here is incipient from a bonding point of view and much weaker than in the typical semibridging situations described by Bénard for a carbonyl dirhodium complex.³²

Yang and co-workers³³ proposed recently a new method of detection and visualization of noncovalent interactions in the real space based on electron density ρ and its derivatives. Highly complementary to analyses based on the QTAIM theory,²⁷ Yang's Non-Covalent Interaction (NCI) region analysis provides an intuitive 3-D isosurface representation³⁴ of local Pauli repulsion, van der Waals interactions, and other local attractive noncovalent interactions like H-bonds.³⁵ This method is based on the strong dependence of the so-called reduced density gradient s on the signed value of the density $\lambda_2\rho$, which allows, by the choice of an appropriate cutoff value for s , to separate noncovalent from covalent interactions, the former being further sorted into either attractive or nonbonded (van der Waals) and repulsive (Pauli) classes depending on the sign of the second electron-density Hessian eigenvalue λ_2 . The sign of the latter is purportedly positive for nonbonded and repulsive interactions, and negative for a range of attractive noncovalent interactions such as H-bonds^{33,34} and the so-called "halogen bonds".³⁵ To the best of our knowledge, there is no report in the literature on the use of Yang's NCI analysis for organometallic systems.

Figure 6 displays NCI region plots for models of **7**,³⁶ **6b**,^{9a} and **4a** where the red-colored isosurfaces are associated with attractive interactions and blue isosurfaces are associated with van der Waals and repulsive interactions for a cutoff value of s of 0.02 au. The red isosurfaces are for the largest part located in the Cr–M segment, while remaining residues materialize

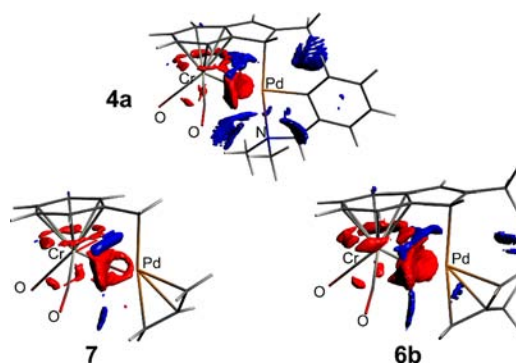


Figure 6. ADFview2013 plots of noncovalent interaction (NCI) regions materialized by *reduced density gradient* isosurfaces (cutoff value $s = 0.02$ au, $\rho = 0.05$ au) colored according to the sign of the signed density $\lambda_2\rho$ (red and blue colors are associated to negatively and positively signed terms) for gas-phase relaxed singlet ground state models of Pd-containing complexes **4a**, **6b**, and **7** (CSDB refcode SOSTID). All calculations were performed with gas phase singlet ground state optimized geometries at the ZORA-PBE0-dDsC/all electron TZP level. Selected distances (in Å) for **7**: Cr–Pd, 2.698 (SOSTID 2.764); Pd–C_{benzylic}, 2.119 (SOSTID 2.103); Pd–C_{CO}, 2.370 (SOSTID 2.639).

attractive NCI regions between the η^6 -arene ligand and the $\text{Cr}(\text{CO})_3$ moiety.

Figure 7 displays a confrontation of the (η^1 -indenyl)platinum isomer **4a'**, written here η^1 -**4a'**, and its parent high-energy (η^3 -

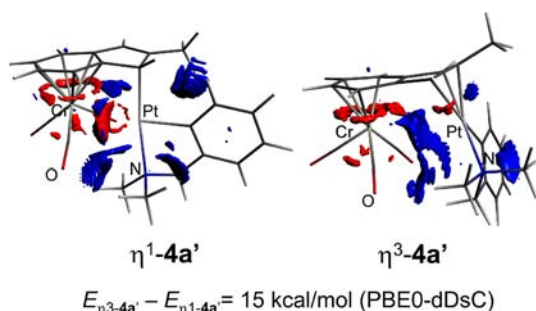


Figure 7. ADFview2013 NCI plots of reduced density gradient isosurfaces (cutoff value $s = 0.02$ au, $\rho = 0.05$ au) colored according to the sign of the signed density $\lambda_2\rho$ (red and blue colors are associated to negatively and positively signed terms) for models of η^1 -**4a'** and η^3 -**4a'**. Calculations were performed at the ZORA-PBE0-dDsC/all electron TZP level with gas phase singlet ground state optimized geometries.

indenyl)platinum singlet ground state fictitious isomer η^3 -**4a'**. It must be noted here that η^3 -**4a'** is by ca. 12 to 15 kcal/mol of total energy (difference of ZPVE, i.e., zero-point vibrational energy, ≈ 0.6 kcal/mol) less stable than η^1 -**4a'** (PBE-D3(BJ) and PBE0-dDsC). The large blue-colored NCI region between the Pt center and the $\text{Cr}(\text{CO})_3$ (Cr–Pt: 3.548 Å) moiety formally denotes a nonbonded interaction ($\lambda_2 > 0$).

2.4. η^1 versus η^3 , Synfacial versus Antarafacial. Early literature on related $\text{Cr}(\text{CO})_3$ -devoid (indenyl)Pd(II)XL complexes tends to suggest a preference for the η^3 bonding mode of coordination to reach valence saturation at Pd.³⁷ The previously outlined importance of noncovalent interactions in the isolated synfacial isomers raises further the question of the nature of the forces that drive the chemical system into such an unusual formally electron-unsaturated situation.

The information on the so-called interaction energy ΔE_{int} obtained by a Ziegler–Rauk energy decomposition analysis (EDA)³⁸ was used to evaluate the benefits gained from a η^1 -synfacial arrangement compared to the η^3 -antarafacial option.⁸ Deformation energies ΔE_{def} were therefore not considered here. According to the general EDA method, the related interaction energies ΔE_{int} were computed for so-called *prepared fragments*, that is for $\text{Cr}(\text{CO})_3$ and 2-methylindenyls substituted with various pertinent metallacycles taken in their geometry in the bonded molecule. The complexes considered thereof are listed in Table 3.

The interaction energy difference $\Delta\Delta E_{\text{int}}$ is introduced here as an evaluation tool of the binding capability of the considered fragments for a given complex relative to a reference case, for example, here compound **1**. For instance, for **4a** $\Delta\Delta E_{\text{int}}(\mathbf{4a}) = \Delta E_{\text{int}}(\mathbf{4a}) - \Delta E_{\text{int}}(\mathbf{1})$. Table 3 lists the corresponding differential EDA subsets of Pauli repulsion ($\Delta\Delta E_{\text{Pauli}}$), attractive electrostatic ($\Delta\Delta E_{\text{electr}}$), attractive dispersion ($\Delta\Delta E_{\text{disp}}$), and orbital ($\Delta\Delta E_{\text{orb}}$) contributions to the interaction energy for optimized singlet ground state models and their associated interacting fragments as treated by ADF's specific *fragment-analysis* routine.³⁹ The η^1 -synfacial bonding interaction is largely favorable with $\Delta\Delta E_{\text{int}} = -30$ kcal/mol (Table 3) in Pd-containing complexes; the situation is similar in **4a'** where $\Delta\Delta E_{\text{int}} = -38$ kcal/mol. Worthy to note, **5b** displays

Table 3. Energy Decomposition Analysis for the Interaction of Prepared Fragments of $\text{Cr}(\text{CO})_3$ and Substituted 2-Methylindenyls Giving Rise to Compounds **4a**, **4a'**, **4b–d**, **4f**, **5b**, and **6a** (Energies Are Expressed in kcal/mol)^a

complex	$\Delta\Delta E_{\text{int}}$	$\Delta\Delta E_{\text{Pauli}}$	$\Delta\Delta E_{\text{electr}}$	$\Delta\Delta E_{\text{disp}}$	$\Delta\Delta E_{\text{orb}}$
4a	-29	64	-59	-6	-29
4a'	-38	137	-106	-6	-63
4b	-29	66	-60	-6	-30
<i>endo-4c</i>	-28	50	-49	-6	-24
<i>exo-4c</i>	-40	45	-43	-6	-37
4d	-30	62	-59	-6	-27
4f	-29	58	-54	-6	-29
5b	0	-14	+6	0	+7
6a	-32	58	-56	-4	-30

^a $\Delta\Delta E_i = \Delta E_i(\text{compound}) - \Delta E_i(\mathbf{1})$; $\Delta E_{\text{interaction}}(\mathbf{1}) = -71.7$ kcal/mol; $\Delta E_{\text{interaction}} = \Delta E_{\text{Pauli}} + \Delta E_{\text{electr}} + \Delta E_{\text{disp}} + \Delta E_{\text{orb}}$.

a value of $\Delta\Delta E_{\text{int}}$ close to zero, which suggests that the presence of the η^3 -bonded metallacycle does not influence much the bonding capability of the indenyl ligand ($\Delta\Delta E_{\text{int}}(\mathbf{5b}) \approx 0$ kcal/mol) toward the $\text{Cr}(\text{CO})_3$ moiety. This analysis shows also that for all η^1 -synfacial heterobimetallics, Pauli repulsion is largely compensated by attractive electrostatic and orbital interactions, dispersion offering a modest contribution at this level of theory.

DFT calculations show in all the cases treated thereof that the synfacial η^1 bonding of the indenyl ligand to the M (M = Pd, Pt) center is largely favored thermodynamically over any synfacial or antarafacial η^3 mode. For instance, **4b** is more stable than complex **5b** by 13.5 kcal/mol of total energy (ZPVE variation ≈ 0.6 kcal/mol). If one performs an EDA analysis by considering now the interaction between prepared anion **2** and the corresponding prepared cationic fluorinated palladacycle, the energetic bias in favor of **4b** appears to result from a major contribution of the Coulombic (electrostatic) attractive energy component of the interaction energy.^{38b} This electrostatic term [$\Delta\Delta E_{\text{electr}}(\mathbf{4b}$ vs $\mathbf{5b}) = -20.5$ kcal/mol] combined to minor dispersion and orbital terms [$\Delta\Delta E_{\text{disp}}(\mathbf{4b}$ vs $\mathbf{5b}) = -6.0$ kcal/mol, $\Delta\Delta E_{\text{orb}}(\mathbf{4b}$ vs $\mathbf{5b}) = -6.2$] largely compensates the Pauli repulsion term ($\Delta\Delta E_{\text{Pauli}}(\mathbf{4b}$ vs $\mathbf{5b}) = +8.8$ kcal/mol) that expectedly rises with increased cluttering. Coulombic attraction appears to be the kernel of the stabilization of those synfacial complexes.

2.5. Acidic Quench of **4c; Production of Enantio-enriched **1**.** The presumed fast equilibrium between the endo and exo diastereomers of **4c** was perceived as a promising property that could be applied to the production of enantio-enriched planar-chiral complex **1** by way of a kinetic chemical quench of the Pd-related transposition process. The latter quench was probed at various temperatures by submitting (**1S**) and (**1R**)-**4c** to an acidic treatment with the goal of protodepalladation of the indenyl ligand and the release of scalemic compound **1**. A temperature-dependent enantiomeric excess (ee) of the latter might express, according to the *Curtin-Hammett* principle, the temperature-dependence of the

Boltzmann distribution of *endo*-4c and *exo*-4c isomers (Figure 9a) in solution.

Proto-depalladation experiments were carried out by treating (1*S*)- and (1*R*)-4c with various sources of protons such as acetic acid (AA), *p*-toluenesulfonic acid (PTSA), or even silica gel (SiO₂) at different temperatures, scalemic **1** being subsequently isolated and purified and its ee determined by the most direct way as described below.

In a first stage, the determination of the respective absolute configuration of the main enantiomers of **1** produced from (1*S*)- and (1*R*)-4c, respectively, by treatment with acetic acid in CH₂Cl₂ at 20 °C was sought. The method suggested by Flack and co-workers was used.⁴⁰ It is based on the combined use of structural X-ray diffraction analyses and spectropolarimetric data (namely absorption UV–visible circular dichroism). The solution CD spectra of freshly prepared batches of scalemic **1** were compared with the CD signatures of solutions obtained by dissolving the enantiopure crystals from which absolute structures were firmly established by structural X-ray diffraction analyses (Figure 8). This procedure that ensures the proper

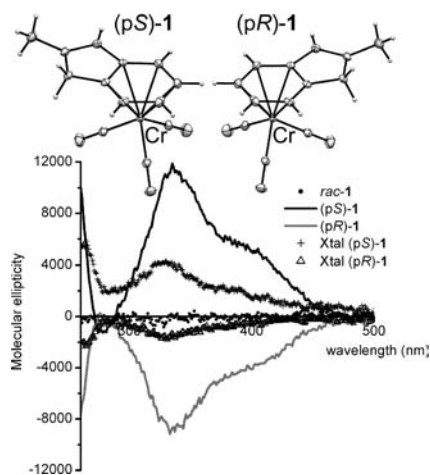


Figure 8. Absolute structures of (p*S*)-**1** (Flack's $x = -0.005(14)$) and (p*R*)-**1** ($x = 0.001(16)$) drawn as thermal ellipsoid-type diagrams at the 30% probability level and the associated circular dichroism (CD) spectra (molecular ellipticity vs wavelength in nm, 10⁻³ M solutions in degassed CH₂Cl₂) of the isolated batches of scalemic compounds (continuous black and gray lines, ee[(p*S*)-**1**] = 13%, ee[(p*R*)-**1**] = 11%, $[\alpha]_D^{25}[(pS)\text{-}1, \text{CH}_2\text{Cl}_2, c\ 0.026] = +346$, $[\alpha]_D^{25}[(pR)\text{-}1, \text{CH}_2\text{Cl}_2, c\ 0.026] = -227$) overlaid with the raw CD signatures (+ and Δ, ordinates are in mdeg) of CH₂Cl₂ solutions of the enantiomeric crystals (Xtal) preliminarily submitted to X-ray diffraction analyses. The flat CD spectrum (dots) of the racemic *rac*-**1** is given as a control reference.

determination of absolute configurations^{40b} was further backed⁴¹ by comparison of the experimental and TDDFT-computed CD spectra of (p*R*)-**1** (ZORA SAOP/all electron QZ4P), which gave a reasonable good match.

It was first concluded that proto-depalladations of (1*S*)-4c and (1*R*)-4c at room temperature mainly yield (p*S*)-**1** and (p*R*)-**1**, respectively.⁴⁰ The enantiomeric excesses of samples of scalemic **1** produced at different temperatures were assessed in all cases by ¹H NMR spectroscopy in the presence of Lacour's Λ-TRISPHAT salt,⁴² which was used here as a chiral shift reagent. Careful integration of the 2-fold split signal of proton H(7) (Figure 9a) gave access to the ee with a reasonable accuracy of ±5%. Under the conditions of chiral shift, proton

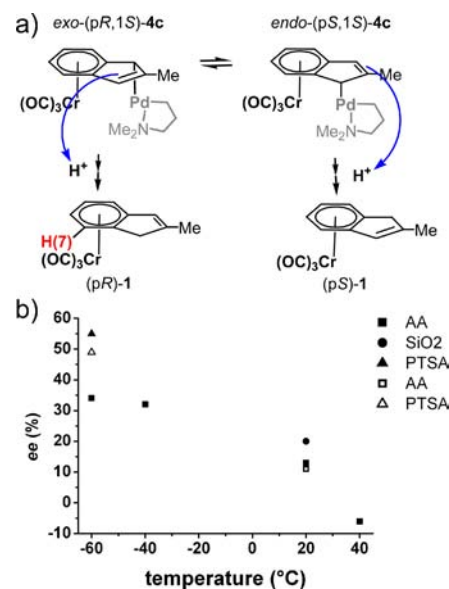


Figure 9. (a) Kinetic quench of the putative endo-exo isomerization by proto-depalladation results from an exo-attack of H⁺ at the indenyl, a pathway established by a reaction of **4a** with CD₃CO₂D, which resulted into the predominant formation of exo-deuterated *rac*-**1** at position 1. (b) ee vs temperature (isolated yields span 30 to 60%), the negative value corresponds to a reversed enantioselectivity; filled and unfilled symbols are for reactions carried out with (1*S*) and (1*R*)-4c, respectively. (Enantiomeric excess ee was calculated for reactions with (1*S*)-4c as follows: ee = 100 × {[p*S*-**1**] - [p*R*-**1**]/([p*R*-**1**] + [p*S*-**1**])} where brackets express concentrations. For reactions with (1*R*)-4c the numerator becomes [p*R*-**1**] - [p*S*-**1**].)

H(7) (Figure 9) shows up as a set of two doublets centered at δ 5.10 ppm ($\Delta\delta(\text{Hz}) = 15$, $T = 298\ \text{K}$, 400 or 600 MHz) when compound **1** is dissolved in a 1:5 mixture of *d*₆-acetone and *d*₆-benzene saturated with Λ-[NBu₃H][TRISPHAT] ($[\alpha]_D^{20} = +299$, EtOH).

On the basis of the absolute configuration of the major product of the reaction and on the structures of diastereomers *endo* and *exo*-4c, it is now speculated that the predominant reaction path that leads to (p*S*)-**1** from (1*S*)-4c consists of the exoprotonation of the indenyl's double bond of endo(p*S*,1*S*)-4c (Figure 9a), which might be the main component of the diastereomeric mixture in solution according to the theoretical analysis of the CD spectrum of (1*S*)-4c (cf., Supporting Information for considerations on the CD spectrum of **4c**). Additional indication of a facial-selectivity of the initial protonation was collected from deuterium-labeling experiments. The deuterolysis of (1*R*)-4c by CD₃CO₂D produced the exo deuterated isomer exo-D-**1** which was isolated in 39% yield. This result has to be compared with the lack of selectivity of the quench of **2** by D₂O that yields exo and endo-D-**1** nearly in a 1:1 ratio (54% isolated yield). Even though the nature of the acid influences slightly the enantioselectivity, the obvious temperature-dependence of the ee (Figure 9), which varies by a factor of about 5 from +20 °C to -60 °C (11–13% < ee < 50–55%, Figure 9b), supports the hypothesis of the fluxional nature of **4c** in solution. Another plausible alternative suggested by a referee could be a temperature-dependent proto-depalladation that could target different sites depending on the temperature at which the reaction is carried out. At the present stage, it was not possible to rule out any of the latter proposals.

3. CONCLUSION

Unprecedented cases of air-stable and solution-persistent neutral T-shaped 14 electron complexes of palladium and platinum have been prepared by a reliable method and extensively structurally characterized. In all cases, a synfacial heterobimetallic complex is the major product, the structure of which is characterized by a Cr–M (M = Pd, Pt) distance of ca. 2.88 Å. The synfacial arrangement in the isolated η^1 -4 complexes (14 + 18 valence electrons) is by more than 10 kcal/mol of total energy preferred over the electron-saturated (16 + 18 valence electrons) antarafacial arrangement in **5** (Scheme 1) and the fictitious synfacial η^3 -4 geometries. This report establishes the feasibility of a permanent stabilization of a coordinatively unsaturated metal center M by noncovalent interactions with vicinal groups. Even though the propensity of arenetricarbonylchromium complexes to form donor–acceptor adducts with Lewis acids is long known,⁴³ in the cases treated here, the donor–acceptor component of the (CO)₃Cr–M interaction revealed by ETS-NOCV analyses is not predominant according to QTAIM.

We propose to name the subtle bonding balance between steric repulsion and electrostatic attraction observed in compounds **4** an *attractive Coulombic occlusion* of a free coordination site (Figure 10).

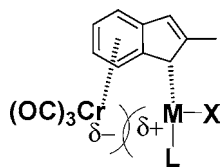


Figure 10. Reductionist representation of the stabilization by *attractive Coulombic occlusion* of the electron-unsaturated M center (M = Pd, Pt) with a proximal large moiety (here Cr(CO)₃) on which charge density concentrates.

The term “chelation” introduced by Morgan and Drew⁴⁴ entails the covalent bonding of a ditopic ligand to a metal center. We propose to name “*hemichelation*” any half-covalent/half-noncovalent bonding-relationship similar to that existing between the ambiphilic heteroditopic tricarbonyl(η^6 -indenyl) chromium ligand and the electron-unsaturated Pd(II) or Pt(II) centers. In line with the observations made for complexes **4** and **6a,b**, the compound synthesized by Kalinin,³⁶ for instance, **7** (vide supra, Figure 3), obviously displays the characteristics of a (η^6 -benzyl)tricarbonylchromium *hemichelate*. Our results also suggest that all situations where similar *hemichelation* might be playing a relevant stabilizing role should warrant extensive investigations. It must be stressed here that the absence of a BCP and bond path between metals, and incidentally the absence of a net metal–metal bond has been pointed out for a number of homometallic bridged transition metal carbonyl dimers and clusters.⁴⁵ This issue has been the subject of a host of reports,⁴⁶ which focused on the relative limitations of QTAIM and on the need for complementary analytical tools^{45b,47} such as the Source Function,⁴⁸ the Electron Localizability Indicator⁴⁹ and the Delocalization Indices⁵⁰ to deepen the analysis of such elusive metal–metal bonding. There is no doubt that the cases reported therein pose a very similar challenge that could be addressed by acquisition of accurate experimental information on the electron density by multipole refinement high resolution structural X-ray diffraction

analysis and subsequent quantum chemical treatment,⁵¹ which was not at reach for the present study. Nonetheless, DFT provides a reasonable insight into the origin of the preference given to the synfacial η^1 -indenyl bonding. Theory outlines the stabilizing nature of the noncovalent interactions existing between chelated M (M = Pd, Pt) and the Cr(CO)₃ moiety and the minor role of direct intermetallic donor–acceptor interactions. The formation of the synfacial arrangement is thermodynamically mostly driven by electrostatic attractive interactions between the M center and the Cr(CO)₃ moiety, which contributes to structural cohesion. Further research on the practical applications of the compounds and concept disclosed here is underway. Further reports on their reactivity will be disclosed elsewhere.

4. EXPERIMENTAL SECTION

4.1. General. All experiments were carried out under a dry argon atmosphere using standard Schlenk techniques or in an argon-filled glovebox. *n*-Butyllithium was purchased from Aldrich Chem. Co as a 1.6 M solution in hexanes. Hexacarbonylchromium was purchased from ABCR. 2-Methyl-1H-indene (98%) was purchased from Aldrich Chem. Co. Celite 545 was purchased from VWR Prolabo. 4-(*t*-Butyl)-2-(*p*-tolyl)pyridine was prepared according to a literature procedure.⁵² The palladacycles used in this study¹⁰ and platinacycle **4a**¹¹ were prepared according to literature procedures. Anhydrous tetrahydrofuran and diethylether were distilled from purple solutions of Na/benzophenone under argon. All other solvents were distilled over sodium or CaH₂ under argon. Deuterated solvents were dried over sodium or CaH₂ and purified by trap-to-trap techniques, degassed by freeze–pump–thaw cycles, and stored under argon. ¹H, ¹³C NMR spectra were obtained on Bruker DPX 300, 400, Avance I 500, and Avance III 600 spectrometers. Chemical shifts (expressed in parts per million) were referenced against solvent peaks or external references. Detailed NMR spectral assignments are provided in the Supporting Information. ¹⁹⁵Pt NMR spectra were referenced against Na₂PtCl₄ in D₂O. Infrared spectra of powdered amorphous samples were acquired with a Fourier transform–IR Bruker alpha spectrometer using an ATR solid state sample cell. Circular dichroism absorption spectropolarimetry was carried out with a UV–visible Jasco J-810 CD spectrometer using a 0.1 mm optical path quartz cell at 20.0 ± 0.1 °C. The determination of specific rotations [α] was performed with a Perkin-Elmer 341 polarimeter at 589 nm (Na) using a thermostatted (20.0 ± 0.1 °C) 10 cm optical path quartz cell.

4.2. Computational Details. Computations were performed with methods of the Density Functional Theory, that is, the Perdew–Burke–Ernzerhof (PBE) GGA functional²⁰ as well as the Tao–Perdew–Staroverov–Scuseria (TPSS) meta-GGA functional⁵³ implemented in the Amsterdam Density Functional package^{39,54} (ADF2013 version) and augmented with Grimme’s DFT-D3(BJ) implementation of dispersion with a Becke–Johnson (BJ) damping function.²¹ The PBE0²⁸-dDsC²⁹ hybrid functional was also used particularly in the perspective of QTAIM and NCI region analyses. Within the PBE scheme electron correlation was treated within the local density approximation (LDA) in the PW92⁵⁵ parametrization. Unless otherwise stated all computations were carried out using scalar relativistic corrections within the Zeroth Order Regular Approximation with ad hoc all-electron (AE) polarized triple- ζ (TZP) Slater-type basis sets. Geometry optimizations by energy gradient-minimization were carried out in all cases with a grid accuracy comprised between 4.5 and 7.5, an energy gradient convergence criterion of 10^{−3} au, and tight to very tight SCF convergence criteria. The COSMO treatment of solvation (with toluene) was applied using the procedure implemented within the ADF package with Klaamt’s adjustment of the van der Waals radii of atoms.⁵⁶ The counterpoise correction for the basis set superposition error (BSSE) was neglected throughout this study. ETS-NOCV analyses, simulations of NMR spectra, and TDDFT computations of CD spectra as well as calculations of vibrational modes were performed with optimized geometries using

Table 4. Acquisition and Refinement Data for the Structures of 4a–b, (1S) and (1R)-4c, 4d–f, 4a', (pR) and (pS)-1

cmpd	4a	4b	5b	(1S)-4c	(1R)-4c
formula	C ₂₂ H ₂₁ CrNO ₃ Pd	C ₂₂ H ₂₀ CrFNO ₃ Pd	C ₂₂ H ₂₀ CrFNO ₃ Pd	C ₂₃ H ₂₃ CrNO ₃ Pd	C ₂₃ H ₂₃ CrNO ₃ Pd
fw	505.80	523.79	523.79	519.82	519.82
cryst habit, color	prism, yellow	plate, orange	prism, orange	prism, red	prism, orange
cryst dim. (mm)	0.20 × 0.18 × 0.12	0.26 × 0.22 × 0.14	0.40 × 0.20 × 0.16	0.22 × 0.20 × 0.18	0.40 × 0.35 × 0.30
cryst syst	monoclinic	monoclinic	monoclinic	monoclinic	monoclinic
space group	P2 ₁ /c	P2 ₁ /c	P2 ₁ /c	P2 ₁	P2 ₁
a (Å)	9.2219(4)	9.144(1) Å	14.8707(6)	9.4903(16)	9.2218(3)
b (Å)	20.3172(7)	20.219(1) Å	8.8067(4)	13.664(2)	13.5560(5)
c (Å)	12.3696(4)	12.4097(9) Å	19.4475(6)	15.769(3)	9.3160(3)
α (deg)	90	90	90	90	90
β (deg)	120.462(2)	119.654(5)°	126.477(2)	90.209 (4)	117.519(1)
γ (deg)	90	90	90	90	90
V (Å ³)	1997.70(13)	1993.8(3)	2047.93(14)	2044.9(6)	1032.83(6)
Z	4	4	4	4	4
ρ (g·cm ⁻³)	1.682	1.745	1.699	1.688	1.671
F (000)	1016	1048	1048	1048	524
T (K)	173	150	173	173	173
θ _{max} (deg)	31.0	30.0	32.0	32.1	32.0
h,k,l range (min/max)	-13/13, -29/13, -17/17	-11/12, -25/28, -16/17	-21/22, -13/10, -29/21	-14/13 -9/20 -23/21	-13/13, -20/20, -13/13
measd reflns	15955	12297	20647	19949	14335
indpt reflns, reflns (I > 2σ(I))	6379, 5303	5689, 5334	7116, 5776	9381, 8591	7006, 6894
params	256	322	276	495	266
R _{int}	0.019	0.022	0.023	0.049	0.013
R ₁	0.023	0.028	0.036	0.071	0.014
wR ₂	0.053	0.085	0.089	0.212	0.037
x (Flack)				0.02(5)	0.018(10)
S	1.02	1.05	1.08	1.06	1.08
cmpd	4d	4f	4a'	(pR)-1	(pS)-1
formula	C ₂₆ H ₂₅ CrFeNO ₃ Pd	C ₂₇ H ₁₇ Cr ₂ NO ₆ Pd 2(CH ₂ Cl ₂)	C ₂₂ H ₂₁ CrNO ₃ Pt	C ₁₃ H ₁₀ CrO ₃	C ₁₃ H ₁₀ CrO ₃
fw	613.72	831.67	594.49	266.21	266.21
cryst habit, color	plate, orange	prism, red	prism, orange	prism, yellow	prism, yellow
cryst dim. (mm)	0.45 × 0.10 × 0.04	0.40 × 0.30 × 0.25	0.40 × 0.26 × 0.10	0.40 × 0.35 × 0.30	0.45 × 0.40 × 0.35
cryst syst	monoclinic	orthorhombic	monoclinic	orthorhombic	orthorhombic
space group	P2 ₁ /c	Pbca	P2 ₁ /c	P2 ₁ 2 ₁ 2 ₁	P2 ₁ 2 ₁ 2 ₁
a (Å)	8.9797(5)	16.4518(6)	9.3081(4)	8.5819(3)	8.5797(3)
b (Å)	18.9572(10)	15.2154(6)	20.2500(8)	10.7371(4)	10.7318(4)
c (Å)	16.0973(7)	24.1031(9)	12.3449(4)	12.1553(5)	12.1582(5)
α (deg)	90	90	90	90	90
β (deg)	121.068(2)	90	121.081(2)	90	90
γ (deg)	90	90	90	90	90
V (Å ³)	2347.2(2)	6033.5(4)	1992.83(13)	1120.05 (7)	1119.47 (7)
Z	4	8	4	4	4
ρ (g·cm ⁻³)	1.737	1.831	1.981	1.579	1.580
F (000)	1232	3296	1144	544	544
T (K)	173	173	173	173	173
θ _{max} (deg)	31.1	31.0	32.0	32.0	32.0
h,k,l range (min/max)	-13/11, -27/15, -20/23	-23/23, -22/17, -34/34	-13/11 -19/30 -17/18	-12/12, -15/15, -17/18	-9/12, -13/16, -12/18
measd reflns	22809	39209	18878	8678	9289
indpt reflns, reflns (I > 2σ(I))	7489, 5470	9552, 7675	6728, 5067	3666, 3430	3770, 3587
params	277	389	5067	155	155
R _{int}	0.047	0.026	0.058	0.017	0.011
R ₁	0.041	0.047	0.040	0.025	0.023
wR ₂	0.090	0.097	0.070	0.069	0.064
x (Flack)				0.001(16)	-0.005(14)
S	1.01	1.15	1.01	1.05	1.05

ADF2013 subroutines. TDDFT calculation were performed from geometries relaxed at the PBE-D3(BJ) level with the model potential SAOP⁵⁷ or with the hybrid functional PBE0 using *ad hoc* all electron ZORA QZ4P basis sets. Vibrational modes were analytically computed to verify that the optimized geometries were related to energy minima: statistical thermodynamic data at 298.15 K were extracted for further determination of enthalpies and variations of Gibbs free enthalpies by conventional methods. Natural population analyses (NPA) as well as Wiberg indice determination were performed with geometries of models relaxed at the (ZORA) PBE-D3(BJ) level using all electron TZP basis sets with the GENNBO²⁴ 5.0 module of ADF. QTAIM and NCI region analyses were carried out using the modules embedded within ADF2013.01. Representations of molecular structures and isosurfaces were produced with ADFview 2013.

4.3. X-ray Diffraction Analyses. Acquisition and processing parameters are displayed in Table 4. Reflections were collected with a Nonius KappaCCD (4b, (1S)-4c) and with an APEX (4a, 5b, (1S)-4c, (1R)-4c, 4d, 4f, 4a', (pR)-1, (pS)-1) diffractometer equipped with an Oxford Cryosystem liquid N₂ device, using Mo K α radiation ($\lambda = 0.71073$ Å). The crystal-detector distance was 38 mm. The cell parameters were determined (APEX2 software⁵⁸) from reflections taken from three sets of 12 frames, each at 10 s exposure. The structures were solved by direct methods using the program SHELXS-97.⁵⁹ The refinement and all further calculations were carried out using SHELXL-97.⁶⁰ The crystal structures acquired with the Nonius Kappa CCD were solved using SIR-97⁶¹ and refined with SHELXL-97.⁶⁰ The refinement and all further calculations were carried out using SHELXL-97.⁶⁰ The H-atoms were included in calculated positions and treated as riding atoms using SHELXL default parameters. The non-H atoms were refined anisotropically, using weighted full-matrix least-squares on F^2 . A semiempirical absorption correction was applied using SADABS in APEX2.⁵⁸

4.4. Standard Procedure for the Synthesis of 4a, 4c, 4d, 4f. Compound 1 was dissolved in diethyl ether (2 mL) and treated with *n*-BuLi at -40 °C under argon. The resulting solution was transferred after 10 min via canula to another Schlenk vessel containing a toluene (3 mL) solution of 3. The resulting solution was stirred for 2 h while the temperature was slowly raised to -10 °C and filtered thrice through Celite to remove palladium black residues. The resulting filtrate was further concentrated to ca. 2 mL, and recrystallizations from a dichloromethane/benzene/pentane mixture of solvents yielded the expected orange solid.

4.5. Synthesis of *cis*-[Tricarbonyl(η^6 -2-methylindenyl)chromium(0), κ^1 , κ^1 {Cr(CO)₃}](*N,N*-dimethyl,phenylene,-methylamine, κ^1 , κ^1 N)palladium(II), 4a. 1 (0.250 g, 0.94 mmol), *n*-BuLi (0.59 mL, 0.94 mmol), 3a (0.259 g, 0.47 mmol): 4a (0.233 g, 49% yield). Calcd for C₂₂H₂₁CrNO₃Pd·0.1CH₂Cl₂: C, 51.61; H, 4.15; N, 2.72. Found: C, 51.67; H, 4.29; N, 2.74. IR ν (CO): 1954 (s), 1877 (s) 1841 (vs) cm⁻¹. ¹H NMR (500 MHz, C₆D₆) δ 7.87 (d, $J = 7.3$ Hz, 1H), 7.28 (t, $J = 7.4$ Hz, 1H), 7.19–7.17 (m, 1H), 7.03 (d, $J = 7.3$ Hz, 1H), 5.55 (s, 1H), 5.23 (d, $J = 6.3$ Hz, 1H), 5.17 (d, $J = 6.6$ Hz, 1H), 4.94 (t, $J = 6.9$ Hz, 1H), 4.45 (s, 1H), 4.10 (t, $J = 6.4$ Hz, 1H), 3.90 (d, $J = 12.9$ Hz, 1H), 2.93 (d, $J = 12.9$ Hz, 1H), 2.41 (s, 3H), 2.34 (s, 3H), 2.15 (d, $J = 1.0$ Hz, 3H). ¹³C NMR (126 MHz, C₆D₆) δ 239.4 (Cr–CO), 237.2 (Cr–CO), 234.1 (Cr–CO), 162.1, 160.2, 147.9, 133.9, 126.1, 124.4, 123.7, 112.1, 107.9, 94.7, 93.4, 90.1, 88.0, 73.9, 51.1, 49.7, 49.5, 18.0. HRMS-ESI (m/z): [M]⁺ calcd for C₂₂H₂₁CrNO₃Pd, 504.9961; found, 504.9956.

4.6. Synthesis of *cis*-[Tricarbonyl(η^6 -2-methylindenyl)chromium(0), κ^1 , κ^1 {Cr(CO)₃}](*N,N*-dimethyl,phenylene,-methylamine, κ^1 , κ^1 N)platinum(II), 4a'. Compounds 3a' (0.282 g, 0.66 mmol) was stirred in chloroform for 13 h in the presence of excess amounts of Me₂S. The reaction mixture was subsequently filtered through Celite, and the filtrate was stripped of solvent under reduced pressure. The resulting light yellow residue was thoroughly dried under reduced pressure and subsequently dissolved in dry toluene (2 mL). The resulting solution was hence treated with a fresh solution of complex 2 prepared from 1 (0.160 g, 0.60 mmol) by treatment with *n*-BuLi (0.41 mL, 0.66 mmol), and the resulting mixture was slowly stirred and warmed from -40 °C to room

temperature in 4 h. The resulting reaction medium was filtered through Celite to remove insoluble materials and strip the solvent. The solid residue was recrystallized from a benzene/pentane mixture to afford orange crystals of compound 4a' (0.043 g, 12% yield). Elem. Anal. Calcd for C₂₂H₂₁CrNO₃Pt·0.3 CH₂Cl₂: C, 43.20; H, 3.51; N, 2.26. Found: C, 43.02; H, 3.80; N, 2.23. IR ν (CO): 1953 (s), 1872 (s), 1818 (s) cm⁻¹. ¹H NMR (600 MHz, C₆D₆) δ 7.95 (dd, $J_{Pt-H} = 75.2$ Hz, $J = 7.5$ Hz, 1H), 7.34–7.27 (m, 1H), 7.24 (t, $J = 7.1$ Hz, 1H), 7.11 (d, $J = 7.2$ Hz, 1H), 5.57–5.47 (m, 2H), 5.36 (d, $J = 6.5$ Hz, 1H), 4.96 (d, $J_{Pt-H} = 134.7$ Hz, 1H), 4.70 (t, $J = 6.5$ Hz, 1H), 4.30 (t, $J = 6.3$ Hz, 1H), 3.78 (d, $J = 12.7$ Hz, 1H), 3.00 (dd, $J_{Pt-H} = 62.0$ Hz, $J = 12.7$ Hz, 1H), 2.49 (s, 3H), 2.46 (s, 3H), 2.16 (s, 3H). ¹³C NMR (126 MHz, C₆D₆) δ 240.9 (Cr–CO), 238.6 (Cr–CO), 236.9 (Cr–CO), 165.8, 155.3, 148.1, 131.3, 126.5, 124.2, 123.5, 117.0, 111.8, 111.5, 94.5, 93.8, 91.8, 91.1, 75.7, 51.9, 50.5, 36.2, 17.6. ¹⁹⁵Pt NMR (86 MHz, *d*₈-toluene) δ -2524.5. HRMS-ESI (m/z): [M+H]⁺ calcd for C₂₂H₂₁CrNO₃Pt, 595.0647; found, 595.0671.

4.7. Synthesis of *cis*-[Tricarbonyl(η^6 -2-methylindenyl)chromium(0), κ^1 , κ^1 {Cr(CO)₃}](*N,N*-dimethyl,3-fluorophenylene,methylamine, κ^1 , κ^1 N)palladium(II), 4b, and [Tricarbonyl(η^6 : η^3 -2-methylindenyl)chromium(0)](*N,N*-dimethyl,phenylene,methylamine, κ^1 , κ^1 N)palladium(II), 5b. 1 (0.200 g, 0.75 mmol) was dissolved in an ether/toluene mixture (2:1, 3 mL) and treated with 1.1 equiv of *n*-BuLi (0.52 mL, 0.83 mmol) at -40 °C under argon. The resulting anion solution was transferred after 10 min via canula to another Schlenk vessel containing a toluene (3 mL) solution of 3b (0.221 g, 0.38 mmol). The resulting solution was stirred 1 h while temperature was slowly raised up to -5 °C and filtered through Celite. The dark red filtrate was concentrated to ca. 2 mL and recrystallization from a CH₂Cl₂/*n*-pentane mixture of solvents gave a pure orange solid (4b, 0.089 g, 23%). The reddish solid retained on the top of the Celite pad was recovered with dichloromethane and recrystallized from *n*-pentane to afford 5b as an orange solid (0.085 g, 22%). (4b) Elem. Anal. Calcd for C₂₂H₂₀CrFNO₃Pd·0.1CH₂Cl₂: C, 49.87; H, 3.82; N, 2.63. Found: C, 49.89; H, 4.01; N, 2.83. IR ν (CO): 1956 (s), 1886 (s), 1847 (vs) cm⁻¹. ¹H NMR (500 MHz, C₆D₆) δ 7.70 (dd, $J = 9.2, 2.4$ Hz, 1H), 6.94–6.76 (m, 2H), 5.48 (s, 1H), 5.14 (d, $J = 6.4$ Hz, 1H), 5.11 (d, $J = 6.6$ Hz, 1H), 4.91 (td, $J = 6.5, 0.9$ Hz, 1H), 4.21 (s, 1H), 4.08 (td, $J = 6.4, 1.0$ Hz, 1H), 3.77 (d, $J = 12.8$ Hz, 1H), 2.86 (d, $J = 12.8$ Hz, 1H), 2.35 (s, 3H), 2.29 (s, 3H), 2.07 (d, $J = 1.1$ Hz, 3H). ¹³C NMR (126 MHz, C₆D₆) δ 239.2 (Cr–CO), 237.0 (Cr–CO), 233.9 (Cr–CO), 163.0, 163.0, 162.5, 161.9, 160.6, 143.4, 143.4, 124.4, 124.4, 120.4, 120.3, 115.2, 112.6, 110.8, 110.6, 107.7, 94.6, 93.4, 90.3, 88.2, 73.2, 73.2, 51.0, 49.5, 49.2, 17.8. ¹⁹F NMR (282 MHz, C₆D₆) δ -116.7. HRMS-ESI (m/z): [M]⁺ calcd for C₂₂H₂₀CrFNO₃Pd, 522.9867; found, 522.9889. (5b) Elem. Anal. Calcd for C₂₂H₂₀CrFNO₃Pd·0.25CH₂Cl₂: C, 49.03; H, 3.79; N, 2.57. Found: C, 48.70; H, 3.95; N, 2.76. IR ν (CO): 1933 (s), 1843 (vs) cm⁻¹. ¹H NMR (500 MHz, C₆D₆) δ 7.33 (dd, $J = 11.1, 2.7$ Hz, 1H), 6.77–6.65 (m, 1H), 6.46 (dd, $J = 7.8, 5.2$ Hz, 1H), 5.00–4.87 (m, 2H, H4), 4.47 (t, $J = 6.1$ Hz, 1H), 4.41 (s, 1H), 4.38 (t, $J = 6.2$ Hz, 1H), 4.02 (s, 1H), 2.82 (d, $J = 13.8$ Hz, 1H), 2.58 (d, $J = 13.4$ Hz, 1H), 2.14 (s, 3H), 1.89 (s, 3H), 1.77 (s, 3H). ¹³C NMR (126 MHz, C₆D₆) δ 236.8 (Cr(CO)₃), 161.6, 159.7, 156.3, 156.3, 143.8, 143.8, 139.1, 127.1, 127.0, 122.7, 122.7, 111.6, 111.4, 108.3, 107.8, 89.2, 88.7, 83.8, 83.3, 83.2, 71.1, 65.7, 54.1, 52.2, 17.4. ¹⁹F NMR (282 MHz, C₆D₆) δ -116.6. HRMS-ESI (m/z): [M]⁺ calcd for C₂₂H₂₀CrFNO₃Pd, 522.9867; found, 522.9924.

4.8. Synthesis of *cis*-[Tricarbonyl(η^6 -2-methylindenyl)chromium(0), κ^1 , κ^1 {Cr(CO)₃}](*N,N*-dimethyl,1-phenylene,-ethylamine, κ^1 , κ^1 N)palladium(II) 4c. 1 (0.200 g, 0.75 mmol), *n*-BuLi (0.52 mL, 0.83 mmol), 3c (0.262 g, 0.45 mmol): 4c (0.233 g, 60%). Elem. Anal. Calcd for C₂₃H₂₃CrNO₃Pd: C, 53.14; H, 4.46; N, 2.69. Found: C, 53.18; H, 4.65; N, 2.69. IR ν (CO): 1941 (s), 1891 (s), 1832 (vs) cm⁻¹. ¹H NMR (500 MHz, C₆D₆) δ 7.79 (d, $J = 7.6$ Hz, 1H), 7.23 (td, $J = 7.4, 1.6$ Hz, 1H), 7.13 (td, $J = 7.4, 1.2$ Hz, 1H), 6.99 (dd, $J = 7.3, 1.5$ Hz, 1H), 5.61 (s, 1H), 5.26 (d, $J = 6.8$ Hz, 1H), 5.18 (d, $J = 6.6$ Hz, 1H), 4.98 (td, $J = 6.5, 0.9$ Hz, 1H), 4.39 (s, 1H), 4.09 (td, $J = 6.4, 1.0$ Hz, 1H), 2.90 (q, $J = 6.4$ Hz, 1H), 2.56 (s, 3H), 2.35 (s, 3H), 2.11 (s, 3H), 1.57 (d, $J = 6.4$ Hz, 3H). ¹³C NMR (126 MHz,

C_6D_6) δ 239.5 (Cr–CO), 237.3 (Cr–CO), 235.1 (Cr–CO), 161.8, 157.0, 155.0, 133.9, 125.9, 124.6, 123.0, 115.7, 111.7, 108.1, 95.0, 93.7, 90.1, 87.7, 77.9, 51.4, 50.8, 47.7, 23.9, 17.8. HRMS-ESI (m/z): $[M]^+$ calcd for $C_{23}H_{23}CrNO_3Pd$, 519.0118; found, 519.0169. (1S)-4c (mixture of diastereomers): $[\alpha]^{20}_D +132.7$ (c 0.052, CH_2Cl_2); +188.5 (c 0.052, benzene). CD (CH_2Cl_2) λ_{max} (Mol. Ellip.) 300 (9012), 330 (–4506), 410 (8405), 470 (–3874); CD (benzene) λ_{max} (Mol. Ellip.) 300 (13750), 330 (–2766), 410 (11009), 470 (–4573). (1R)-4c (mixture of diastereomers): $[\alpha]^{20}_D -167.3$ (c 0.052, CH_2Cl_2); $[\alpha]^{20}_D -244.2$ (c 0.052, benzene). CD (CH_2Cl_2) λ_{max} (Mol. Ellip.) 300 (–12811), 330 (3510), 410 (–11483), 470 (4078); CD (benzene) λ_{max} (Mol. Ellip.) 300 (–17554), 330 (2527), 410 (–13498), 470 (4113).

4.9. Synthesis of *cis*-[Tricarbonyl(η^6 -2-methylindenyl)-chromium(0), $\kappa C^1, \kappa\{Cr(CO)_3\}$](*N,N*-dimethylferrocenylene-methylamine, $\kappa C^1, \kappa N$)palladium(II), 4d. 1 (0.200 g, 0.75 mmol), *n*-BuLi (0.52 mL, 0.83 mmol), 3d (0.346 g, 0.45 mmol): 4d (0.397 g, 86% yield). Elem. Anal. Calcd for $C_{26}H_{25}CrFeNO_3Pd$: C, 50.88; H, 4.11; N, 2.28. Found: C, 50.97; H, 4.37; N, 2.26. IR ν (CO): 1941(s), 1872(s), 1843(vs) cm^{-1} . 1H NMR (500 MHz, C_6D_6) δ 5.80–5.71 (m, 1H), 5.60 (s, 1H), 5.22 (d, J = 6.7 Hz, 1H), 5.00 (td, J = 6.6, 0.9 Hz, 1H), 4.86 (s, 1H), 4.39 (dd, J = 2.1, 0.8 Hz, 1H), 4.35 (td, J = 6.4, 1.0 Hz, 1H), 4.27 (s, 5H), 4.21–4.17 (m, 1H), 4.16 (t, J = 2.2 Hz, 1H), 4.03 (d, J = 13.0 Hz, 1H), 2.51 (d, J = 13.0 Hz, 1H), 2.40 (d, J = 1.1 Hz, 3H), 2.37 (s, 3H), 2.24 (s, 3H). ^{13}C NMR (126 MHz, C_6D_6) δ 238.9 (Cr–CO), 238.1 (Cr–CO), 234.8 (Cr–CO), 160.3, 116.7, 112.0, 107.5, 106.7, 94.8, 94.3, 93.3, 91.8, 88.5, 70.2 (5C), 70.0, 67.5, 66.8, 64.1, 51.0, 50.5, 45.5, 17.9. HRMS-ESI (m/z): $[M]^+$ calcd for $C_{26}H_{25}CrFeNO_3Pd$, 612.9624; found, 612.9593.

4.10. Synthesis of 3e. A mixture containing palladium(II) chloride (1.0 g, 5.64 mmol), potassium chloride (0.841 g, 11.28 mmol), and 4-(*t*-butyl)-2-(*p*-tolyl)pyridine⁵² (3.81 g, 16.92 mmol) in 50 mL of degassed methanol was refluxed under argon for 36 h. After the solutions was cooled to room temperature, the resulting white suspension was filtered and washed with cold methanol and pentane, and eventually dried under reduced pressure to afford off white-colored compound 3e (1.875 g, 91% yield). Elem. Anal. Calcd for $C_{32}H_{36}Cl_2N_2Pd_2$: C, 52.48; H, 4.95; N, 3.82. Found: C, 52.31; H, 5.10; N, 3.80. 1H NMR (500 MHz, C_6D_6 + 1 drop of pyridine) δ 9.93 (d, J = 6.1 Hz, 1H), 7.38 (s, 1H), 7.37 (d, J = 6.4 Hz, 1H), 6.94–6.87 (m, 1H), 6.44 (dd, J = 6.2, 2.1 Hz, 1H), 6.31 (s, 1H), 2.05 (s, 3H), 0.93 (s, 9H). ^{13}C NMR (126 MHz, C_6D_6 + 1 drop of pyridine) δ 165.9, 162.7, 156.9, 152.6, 144.2, 139.3, 134.1, 125.5, 123.4, 119.2, 114.7, 34.9, 30.0 (3C), 21.9. HRMS-ESI (m/z): $[M+H]^+$ calcd for $C_{32}H_{36}Cl_2N_2Pd_2$, 731.0398; found, 731.0451.

4.11. Synthesis of *cis*-[Tricarbonyl(η^6 -2-methylindenyl)-chromium(0), $\kappa C^1, \kappa\{Cr(CO)_3\}$](1-(3-methylphenylene)-4-*t*-butylpyridine, $\kappa C^1, \kappa N$)palladium(II), 4e. Compound 1 (0.200 g, 0.75 mmol) was dissolved in tetrahydrofuran (THF) (5 mL) and treated with *n*-BuLi (0.52 mL, 0.83 mmol) at -40 °C under argon. The resulting solution was transferred after 10 min via canula to another Schlenk vessel containing 0.7 equiv of 3e (0.385 g, 0.53 mmol). The solution was stirred for 3 h while temperature was slowly raised to room temperature. Chilled toluene (5 mL) was added to the solution and the resulting suspension was filtered through Celite to remove residues of palladium black. The filtrate was further concentrated to ca. 2 mL and *n*-pentane was added to induce precipitation. The supernatant was removed and evaporation of the solvents under reduced pressure afforded 4e as an orange solid (0.280 g, 63% yield), which displayed low solubility in almost all common solvents. Elem. Anal. Calcd for $C_{29}H_{27}CrNO_3Pd \cdot 0.6CH_2Cl_2$: C, 54.96; H, 4.39; N, 2.17. Found: C, 54.98; H, 4.60; N, 2.19. IR ν (CO): 1948(s), 1887(s), 1843(vs) cm^{-1} . 1H NMR (500 MHz, $CDCl_3$) δ 8.25 (d, J = 6.0 Hz, 1H), 7.79 (s, 1H), 7.72 (d, J = 1.8 Hz, 1H), 7.62 (d, J = 7.9 Hz, 1H), 7.06 (dd, J = 6.1, 2.1 Hz, 1H), 7.02 (d, J = 7.9 Hz, 1H), 6.04 (d, J = 6.4 Hz, 1H), 5.96 (d, J = 6.5 Hz, 1H), 5.88 (t, J = 6.5 Hz, 1H), 5.79 (s, 1H), 5.14–5.06 (m, 1H), 4.71 (s, 1H), 2.47 (s, 3H), 2.40–2.37 (m, 3H), 1.33 (s, 11H). ^{13}C NMR (126 MHz, $CDCl_3$) δ 241.4 (Cr–CO), 237.6 (Cr–CO), 233.4 (Cr–CO), 165.1, 162.9, 162.0, 161.7, 152.7, 144.7, 139.6, 135.7, 125.3, 124.2, 119.6, 115.5, 115.4,

112.6, 108.4, 95.2, 93.5, 90.1, 88.1, 50.5, 35.3, 30.5, 22.2, 17.7. HRMS-ESI (m/z): $[M+H]^+$ calcd for $C_{29}H_{27}CrNO_3Pd$, 596.0504; found, 596.0506.

4.12. Synthesis of *cis*-[Tricarbonyl(η^6 -2-methylindenyl)-chromium(0), $\kappa C^1, \kappa\{Cr(CO)_3\}$][1-(tricarbonyl(η^6 -phenylene)-chromium)pyridine, $\kappa C^1, \kappa N$]palladium(II), 4f. 1 (0.200 g, 0.56 mmol), *n*-BuLi (0.35 mL, 0.56 mmol), 3f (0.248 g, 0.29 mmol): 4f (0.203 g, 54% yield). Elem. Anal. Calcd for $C_{27}H_{17}Cr_2NO_6Pd \cdot 1.25CH_2Cl_2$: C, 44.18; H, 2.56; N, 1.82. Found: C, 44.03; H, 2.92; N, 1.72. IR ν (CO): 1974 (s), 1940 (s), 1911 (s), 1876 (vs), 1851 (vs) cm^{-1} . 1H NMR (500 MHz, C_6D_6) δ 8.47 (d, J = 4.9 Hz, 1H), 6.64 (t, J = 7.7 Hz, 1H), 6.55 (d, J = 7.8 Hz, 1H), 6.13 (t, J = 6.4 Hz, 1H), 5.95 (d, J = 6.5 Hz, 1H), 5.63 (d, J = 6.2 Hz, 1H), 5.54 (s, 1H), 5.24 (d, J = 6.7 Hz, 1H), 5.14–5.06 (m, 2H), 4.93 (t, J = 6.4 Hz, 1H), 4.68–4.58 (m, 1H), 4.28 (s, 1H), 4.18 (t, J = 6.1 Hz, 1H), 2.23 (d, J = 1.9 Hz, 3H). ^{13}C NMR (126 MHz, C_6D_6) δ 238.3 (Cr–CO), 236.7 (Cr–CO), 234.8 (Cr(CO)₃), 233.6 (Cr–CO), 163.1, 159.8, 153.2, 137.7, 127.5, 123.0, 118.1, 114.3, 114.2, 111.1, 108.0, 96.4, 96.3, 95.1, 93.5, 92.7, 90.9, 89.2, 88.9, 49.6, 17.3. HRMS-ESI (m/z): $[M+H]^+$ calcd for $C_{27}H_{17}Cr_2NO_6Pd$, 661.8974; found, 661.9021.

4.13. Typical Procedure for the Preparation of Compounds (pR)-1 and (pS)-1 by Proto-demetalation of 4c in the Presence of Acetic Acid. A solution of (1R)-4c or (1S)-4c (0.100 g, 0.09 mmol) and acetic acid (0.1 mL, 1.73 mmol) in dry dichloromethane (2 mL) was stirred under argon at room temperature during 15 min. The solvent was then removed under vacuo, and the residue was treated by flash chromatography on silica gel using a mixture of CH_2Cl_2 and pentane (5:5) as eluent. The product was recovered as a yellow-colored powder upon removal of the solvents under reduced pressure (cf. Supporting Material for information on ee).

4.14. Benzylic Deuteration of 1. Compound 1 (0.200 g, 0.75 mmol) was dissolved in diethyl ether (2 mL) and treated with 1.1 equiv of *n*-BuLi (0.52 mL, 0.83 mmol) at -40 °C under argon. Deuterium oxide (0.30 mL, 15 mmol) was added after 10 min to the resulting anion solution, and the reaction mixture was stirred during 3 h while temperature was warmed to 0 °C. Solvent was then removed under vacuum and the resulting residue was purified by silica gel column chromatography using a mixture of CH_2Cl_2 and pentane (1:1) as eluent. Evaporation of the yellow band led to the pure solid-state compound *d*₁-1 (107 mg, 54% yield), which was analyzed by 1H NMR spectroscopy.

4.15. Deutero-depalladation of (1R)-4c. Compound (1R)-4c (10 mg, 0.02 mmol), CD_3CO_2D (0.01 mL, 0.15 mmol) in dry dichloromethane (2 mL) was stirred under argon at room temperature during 30 min. The solvent was then removed under reduced pressure. The residue was dissolved in a minimum amount of CH_2Cl_2 and eluted through a short column of silica gel with a mixture of CH_2Cl_2 and pentane (1:1). The yellow band containing *d*₁-1 was recovered, evaporated to dryness (2 mg, 39% yield), and further analyzed by 1H NMR.

■ ASSOCIATED CONTENT

📄 Supporting Information

Experimental MS and NMR spectra with detailed assignments, crystallographic CIF data and X-ray diffraction geometries of the main complexes, Cartesian coordinates of singlet ground state relaxed geometries, energies, vibrational frequencies, and computed CD spectra of considered models. This material is available free of charge via the Internet at <http://pubs.acs.org>.

■ AUTHOR INFORMATION

Corresponding Author

djukic@unistra.fr.

Notes

The authors declare no competing financial interest.

ACKNOWLEDGMENTS

This work was funded by the funds of the ANR (projet blanc 2010 WEAKINTERMET-2DA) and LABEX "Chimie des Systèmes Complexes". The authors thank the CNRS and the University of Strasbourg for their financial contribution, M. Pfeffer for his expertise, Frédéric La Paglia for his technical assistance, Bruno Vincent, Lionel Allouche and Mélanie Lebreton for their contribution to NMR and MS characterizations.

REFERENCES

- (1) (a) Alvarez, R.; Faza, O. N.; de Lera, A. R.; Cardenas, D. J. *Adv. Synth. Catal.* **2007**, *349*, 887–906. (b) Sergeev, A. G.; Spannenberg, A.; Beller, M. J. *Am. Chem. Soc.* **2008**, *130*, 15549–15563.
- (2) Marrone, A.; Re, N.; Romeo, R. *Organometallics* **2008**, *27*, 2215–2222.
- (3) (a) Jensen, W. B. *J. Chem. Educ.* **2005**, *82*, 28. (b) Langmuir, I. *Science* **1921**, *54*, 59–67. (c) Pyykkö, P. *J. Organomet. Chem.* **2006**, *691*, 4336–4340.
- (4) (a) Urtel, H.; Meier, C.; Eisenträger, F.; Rominger, F.; Joschek, J. P.; Hofmann, P. *Angew. Chem., Int. Ed.* **2001**, *40*, 781–784. (b) Rivada-Wheelaghan, O.; Ortuno, M. A.; Diez, J.; Lledos, A.; Conejero, S. *Angew. Chem., Int. Ed. Engl.* **2012**, *51*, 3936–3939. (c) Crosby, S. H.; Clarkson, G. J.; Rourke, J. P. *J. Am. Chem. Soc.* **2009**, *131*, 14142–14143. (d) Ara, I.; Fornies, J.; Garcia, A.; Gomez, J.; Lalinde, E.; Moreno, M. T. *Chem.—Eur. J.* **2002**, *8*, 3698–3716. (e) Braunschweig, H.; Gruss, K.; Radacki, K. *Angew. Chem., Int. Ed.* **2007**, *46*, 7782–7784. (f) Walter, M. D.; White, P. S.; Brookhart, M. *New J. Chem.* **2013**, *37*, 1128–1133. (g) Baratta, W.; Stoccoro, S.; Doppiu, A.; Herdtweck, E.; Zucca, A.; Rigo, P. *Angew. Chem., Int. Ed.* **2003**, *42*, 105–109.
- (5) (a) Stambuli, J. P.; Incarvito, C. D.; Bühl, M.; Hartwig, J. F. *J. Am. Chem. Soc.* **2004**, *126*, 1184–1194. (b) Stambuli, J. P.; Weng, Z.; Incarvito, C. D.; Hartwig, J. F. *Angew. Chem., Int. Ed.* **2007**, *46*, 7674–7677. (c) Yandulov, D. V.; Tran, N. T. *J. Am. Chem. Soc.* **2007**, *129*, 1342–1358. (d) Perez-Rodriguez, M.; Braga, A. A. C.; de Lera, A. R.; Maseras, F.; Alvarez, R.; Espinet, P. *Organometallics* **2010**, *29*, 4983–4991. (e) Gerber, R.; Blacque, O.; Frech, C. M. *Dalton Trans.* **2011**, *40*, 8996–9003.
- (6) (a) Clegg, W.; Eastham, G. R.; Elsegood, M. R. J.; Heaton, B. T.; Iggo, J. A.; Tooze, R. P.; Whyman, R.; Zacchini, S. *Organometallics* **2002**, *21*, 1832–1840. (b) Ingleson, M. J.; Mahon, M. F.; Weller, A. S. *Chem. Commun.* **2004**, 2398–2399. (c) Braunschweig, H.; Radacki, K.; Rais, D.; Scheschke, D. *Angew. Chem., Int. Ed.* **2005**, *44*, 5651–5654. (d) Kefalidis, C. E.; Tsipis, C. A. *J. Comput. Chem.* **2012**, *33*, 1689–1700.
- (7) (a) Fox, B. J.; Sun, Q. Y.; di Pasquale, A. G.; Fox, A. R.; Rheingold, A. L.; Figueroa, J. S. *Inorg. Chem.* **2008**, *47*, 9010–9020. (b) Labios, L. A.; Millard, M. D.; Rheingold, A. L.; Figueroa, J. S. *J. Am. Chem. Soc.* **2009**, *131*, 11318–11319. (c) Margulieux, G. W.; Weidemann, N.; Lacy, D. C.; Moore, C. E.; Rheingold, A. L.; Figueroa, J. S. *J. Am. Chem. Soc.* **2010**, *132*, 5033–5035. (d) Emerich, B. M.; Moore, C. E.; Fox, B. J.; Rheingold, A. L.; Figueroa, J. S. *Organometallics* **2011**, *30*, 2598–2608. (e) Lewis, R. A.; George, S. P.; Chapovetsky, A.; Wu, G.; Figueroa, J. S.; Hayton, T. W. *Chem. Commun.* **2013**, *49*, 2888–2890.
- (8) Hyla-Kryspin, I.; Grimme, S.; Djukic, J.-P. *Organometallics* **2009**, *28*, 1001–1013.
- (9) (a) Werlé, C.; Hamdaoui, M.; Bailly, C.; Le Goff, X.-F.; Brelot, L.; Djukic, J.-P. *J. Am. Chem. Soc.* **2013**, *135*, 1715–1718. (b) Schwabe, T.; Grimme, S.; Djukic, J.-P. *J. Am. Chem. Soc.* **2009**, *131*, 14156–14157. (c) Grimme, S.; Djukic, J.-P. *Inorg. Chem.* **2010**, *49*, 2911–2919. (d) Grimme, S.; Djukic, J.-P. *Inorg. Chem.* **2011**, *50*, 2619–2628.
- (10) (a) Cope, A. C.; Friedrich, E. C. *J. Am. Chem. Soc.* **1968**, *90*, 909–913. (b) Ryabov, A. D.; van Eldik, R.; Borgne, G. L.; Pfeffer, M. *Organometallics* **1993**, *12*, 1386–1393. (c) Otsuka, S.; Nakamura, A.; Kano, T.; Tani, K. *J. Am. Chem. Soc.* **1971**, *93*, 4301–4303. (d) Gaunt, J. C.; Shawn, B. L. *J. Organomet. Chem.* **1975**, *102*, 511–516.
- (e) Berger, A.; de Cian, A.; Djukic, J.-P.; Fischer, J.; Pfeffer, M. *Organometallics* **2001**, *20*, 3230–3240.
- (11) (a) Cope, A. C.; Friedrich, E. C. *J. Am. Chem. Soc.* **1968**, *90*, 909–913. (b) Schmuelling, M.; Ryabov, A. D.; Van, E. R. *J. Chem. Soc., Chem. Commun.* **1992**, 1609–1611.
- (12) Thomas, S. W.; Venkatesan, K.; Muller, P.; Swager, T. M. *J. Am. Chem. Soc.* **2006**, *128*, 16641–16648.
- (13) Slater, J. C. *J. Chem. Phys.* **1964**, *41*, 3199–3204.
- (14) (a) Adams, D. M.; Squire, A. *J. Chem. Soc., Dalton Trans.* **1974**, 558–565. (b) Neuse, E. W. *J. Organomet. Chem.* **1975**, *99*, 287–295. (c) Van Meurs, F.; Baas, J. M. A.; Van Bekkum, H. *J. Organomet. Chem.* **1976**, *113*, 353–359. (d) Van Meurs, F.; Baas, J. M. A.; Van Bekkum, H. *J. Organomet. Chem.* **1977**, *129*, 347–360.
- (15) Van Lenthe, E.; Baerends, E. J. *J. Comput. Chem.* **2003**, *24*, 1142–1156.
- (16) (a) Djukic, J.-P.; Pfeffer, M.; Dotz, K. H. *C. R. Acad. Sci., Ser. IIC: Chim.* **1999**, *2*, 403–408. (b) Djukic, J.-P.; Maise-Francois, A.; Pfeffer, M.; Doetz, K. H.; De Cian, A.; Fischer, J. *Organometallics* **2000**, *19*, 5484–5499. (c) Djukic, J.-P.; Michon, C.; Maise-Francois, A.; Allagapen, R.; Pfeffer, M.; Dotz, K. H.; De Cian, A.; Fischer, J. *Chem.—Eur. J.* **2000**, *6*, 1064–1077.
- (17) Sandstrom, J. *Dynamic NMR Spectroscopy*; Academic Press: New York, 1982.
- (18) Deverell, C.; Morgan, R. E.; Strange, J. H. *Mol. Phys.* **1970**, *18*, 553–559.
- (19) Schlögl, K. *Top. Stereochem.* **1967**, *1*, 39–91.
- (20) Perdew, J. P.; Burke, K.; Ernzerhof, M. *Phys. Rev. Lett.* **1996**, *77*, 3865–3868.
- (21) (a) Grimme, S.; Antony, J.; Ehrlich, S.; Krieg, H. *J. Chem. Phys.* **2010**, *132*, 154104. (b) Grimme, S.; Ehrlich, S.; Goerigk, L. *J. Comput. Chem.* **2011**, *32*, 1456–1465.
- (22) Staroverov, V. N.; Scuseria, G. E.; Tao, J.; Perdew, J. P. *J. Chem. Phys.* **2003**, *119*, 12129.
- (23) Steinmann, S. N.; Piemontesi, C.; Delachat, A.; Corminboeuf, C. *J. Chem. Theor. Comp.* **2012**, *8*, 1629–1640.
- (24) Weinhold, F. In *Encyclopedia of Computational Chemistry*; von Ragué-Schleyer, P., Allinger, N. L., Clark, T., Gasteiger, J., Kollman, P. A., Schaefer, H. F., Schreiner, P. R., Eds.; John Wiley & Sons: Chichester, UK, 1998; Vol. 3, pp 1792–1811.
- (25) Weinhold, F.; Landis, C. R. *Valency and Bonding, a Natural Bond Orbital Donor-Acceptor Perspective*; University Press: Cambridge, UK, 2005.
- (26) (a) Mitoraj, M. P.; Michalak, A.; Ziegler, T. *Organometallics* **2009**, *28*, 3727–3733. (b) Mitoraj, M. P.; Michalak, A.; Ziegler, T. *J. Chem. Theory Comput.* **2009**, *9*, 962–975.
- (27) (a) Bader, R. F. W. In *Atoms in Molecules: A Quantum Theory*; Clarendon: Oxford, 1990. (b) Popelier, P. *Atoms in Molecules, An Introduction*; Prentice Hall: Harlow, England, 2000.
- (28) (a) Ernzerhof, M.; Scuseria, G. E. *J. Chem. Phys.* **1999**, *110*, 5029–5036. (b) Adamo, C.; Barone, V. *J. Chem. Phys.* **1999**, *110*, 6158.
- (29) Steinmann, S. N.; Corminboeuf, C. *J. Chem. Theor. Comp.* **2011**, *7*, 3567–3577.
- (30) Macchi, P.; Garlaschelli, L.; Martinengo, S.; Sironi, A. *J. Am. Chem. Soc.* **1999**, *121*, 10428–10429.
- (31) Bo, C.; Sarasa, J. P.; Poblet, J. M. *J. Phys. Chem.* **1993**, *97*, 6362–6366.
- (32) Bo, C.; Costas, M.; Poblet, J. M.; Rohmer, M.-M.; Benard, M. *Inorg. Chem.* **1996**, *35*, 3298–3306.
- (33) Johnson, E.; Keinan, S.; Mauri-Sanchez, P.; Contreras-Garcia, J.; Cohen, A. J.; Yang, W. *J. Am. Chem. Soc.* **2010**, *132*, 6498–6506.
- (34) Contreras-Garcia, J.; Johnson, E. R.; Keinan, S.; Chaudret, R.; Piquemal, J. P.; Beratan, D. N.; Yang, W. *J. Chem. Theor. Comput.* **2011**, *7*, 625–632.
- (35) Johansson, M. P.; Swart, M. *Phys. Chem. Chem. Phys.* **2013**, *15*, 11543–11553.
- (36) (a) Kalinin, V. N.; Cherepanov, I. A.; Moiseev, S. K.; Batsanov, A. S.; Struchkov, Y. T. *Mendeleev Commun.* **1991**, 77–78. (b) Kalinin, V. N.; Cherepanov, I. A.; Moiseev, S. K.; Dolgushin, F. M.; Yanovsky,

A. I.; Struchkov, Y. T. *Acta Crystallogr., Sect. C: Cryst. Struct. Commun.* **1993**, *C49*, 805–808. (c) Moiseev, S. K.; Cherepanov, I. A.; Petrovskii, P. V.; Ezernitskaya, M. G.; Butenschoen, H.; Strotmann, M.; Kalinin, V. N. *Inorg. Chim. Acta* **1998**, *280*, 71–74.

(37) (a) Bielinski, E. A.; Dai, W.; Guard, L. M.; Hazari, N.; Takase, M. K. *Organometallics* **2013**, *32*, 4025–4037. (b) Chalkley, M. J.; Guard, L. M.; Hazari, N.; Hofmann, P.; Hruszkewycz, D. P.; Schmeier, T. J.; Takase, M. K. *Organometallics* **2013**, *32*, 4223–4238. (c) Sui-Seng, C.; Enright, G. D.; Zargarian, D. *Organometallics* **2004**, *23*, 1236–1246. (d) Sui-Seng, C.; Enright, G. D.; Zargarian, D. *J. Am. Chem. Soc.* **2006**, *128*, 6508–6519. (e) Alias, F. M.; Belderrain, T. R.; Paneque, M.; Poveda, M. L.; Carmona, E.; Valerga, P. *Organometallics* **1998**, *17*, 5620–5629.

(38) (a) Bickelhaupt, F. M.; Baerends, E. J.; Lipkowitz, K. B.; Boyd, D. B., Eds.; Wiley: New York, 2000; Vol. 15, pp 1–86. (b) Ziegler, T.; Rauk, A. *Inorg. Chem.* **1979**, *18*, 1755–1759.

(39) te Velde, G.; Bickelhaupt, F. M.; Baerends, E. J.; Fonseca Guerra, C.; van Gisbergen, S. J. A.; Snijders, J. G.; Ziegler, T. *J. Comput. Chem.* **2001**, *22*, 931–967.

(40) (a) Flack, H. D.; Bernardinelli, G. *Acta Crystallogr., Sect. A: Found. Crystallogr.* **1999**, *A55*, 908–915. (b) Djukic, J.-P.; Hijazi, A.; Flack, H. D.; Bernardinelli, G. *Chem. Soc. Rev.* **2008**, *37*, 406–425.

(41) Pescitelli, G.; Kurtán, T.; Flörke, U.; Krohn, K. *Chirality* **2009**, *21*, E181–E201.

(42) (a) Lacour, J. C. R. *Chim.* **2010**, *13*, 985–997. (b) Favarger, F.; Goujon-Ginglinger, C.; Monchaud, D.; Lacour, J. *J. Org. Chem.* **2004**, *69*, 8521–8524. (c) Lacour, J. *Chimia* **2002**, *56*, 672–675.

(43) (a) Edgar, K.; Johnson, B. F. G.; Lewis, J.; Wild, S. B. *J. Chem. Soc. A* **1968**, 2851–2855. (b) Magomedov, G. I.; Syrkin, V. G.; Frenkel, A. S.; Zakharchenko, O. A. *Zh. Obshch. Khim.* **1975**, *45*, 2530–2533. (c) Lokshin, B. V.; Rusach, E. B.; Kolobova, N. E.; Makarov, Y. V.; Ustynyuk, N. A.; Zdanovich, V. I.; Zhakaeva, A. Z.; Setkina, V. N. *J. Organomet. Chem.* **1976**, *108*, 353–361.

(44) Morgan, G. T.; Drew, H. D. K. *J. Chem. Soc., Trans.* **1920**, 117, 1456–1465.

(45) (a) Farrugia, L. J. *Chem. Phys. Lett.* **2005**, *414*, 122–126. (b) Farrugia, L. J.; Senn, H. M. *J. Phys. Chem. A* **2010**, *114*, 13418–13433.

(46) Gervasio, G.; Bianchi, R.; Marabello, D. *Chem. Phys. Lett.* **2005**, *407*, 18–22.

(47) Overgaard, J.; Clausen, H. F.; Platts, J. A.; Iversen, B. B. *J. Am. Chem. Soc.* **2008**, *130*, 3834–3843.

(48) Bader, R. F. W.; Gatti, C. *Chem. Phys. Lett.* **1998**, *287*, 233–238.

(49) Kohout, M. *Int. J. Quantum Chem.* **2004**, *97*, 651–658.

(50) Fradera, X.; Austen, M. A.; Bader, R. F. W. *J. Phys. Chem. A* **1998**, *103*, 304–314.

(51) Gatti, C. Z. *Kristallogr.* **2005**, *220*, 399–457.

(52) Djukic, J.-P.; Parkhomenko, K.; Hijazi, A.; Chemmi, A.; Allouche, L.; Brelot, L.; Pfeffer, M.; Ricard, L.; Le Goff, X.-F. *Dalton Trans.* **2009**, 2695–2711.

(53) Tao, J.; Perdew, J. P.; Staroverov, V. N.; Scuseria, G. E. *Phys. Rev. Lett.* **2003**, *91*, 146401.

(54) Brown, D. A.; Fitzpatrick, N. J.; Glass, W. K.; Ahmed, H. A.; Cunningham, D.; McArdle, P. J. *Organomet. Chem.* **1993**, *455*, 157–166.

(55) Perdew, J. P.; Wang, Y. *Phys. Rev. B* **1992**, *45*, 13244–13249.

(56) Klamt, A.; Schuurmann, G. *J. Chem. Soc., Perkin Trans. 2* **1993**, 799–805.

(57) Gritsenko, O. V.; Schipper, P. R. T.; Baerends, E. J. *Chem. Phys. Lett.* **1999**, *302*, 199–207.

(58) In *M86-E01078 APEX2 User Manual*; Bruker AXS Inc.: Madison, USA, 2006.

(59) Sheldrick, G. M. *Acta Crystallogr., Sect. B* **1990**, *A46*, 467–473.

(60) Sheldrick, M.; Universität Göttingen: Göttingen, Germany, 1998.

(61) Altomare, A.; Burla, M. C.; Camalli, M.; Cascarano, G.; Giacovazzo, C.; Guagliardi, A.; Moliterni, A. G. G.; Polidori, G.; Spagna, R. *J. Appl. Cryst.* **1999**, *32*, 115–119.